# Intra-event evolution of elemental and ionic concentrations in wet deposition in an urban environment

Thomas Audoux, Benoit Laurent, Karine Desboeufs, Gael Noyalet, Franck Maisonneuve, Olivier Lauret, Servanne Chevaillier

Atmos. Chem. Phys., 23, 13485–13503, 2023
https://doi.org/10.5194/acp-23-13485-2023


Atmospheric Chemistry and Physics
Open Access
EGU

Research article

# Intra-event evolution of elemental and ionic concentrations in wet deposition in an urban environment

**Thomas Audoux**[1], **Benoit Laurent**[1], **Karine Desboeufs**[1], **Gael Noyalet**[1], **Franck Maisonneuve**[2], **Olivier Lauret**[2,3], and **Servanne Chevaillier**[2]

[1]Université Paris Cité and Université Paris-Est Créteil , CNRS, LISA, 75013, Paris, France
[2]Université Paris-Est Créteil and Université Paris Cité, CNRS, LISA, 94010, Créteil, France
[3]Université Paris-Est Créteil , CNRS, ENPC, Université Paris Cité, OSU-EFLUVE, 94010, Créteil, France

**Correspondence:** Thomas Audoux (thomas.audoux@lisa.ipsl.fr) and Benoit Laurent (benoit.laurent@lisa.ipsl.fr)

Received: 16 May 2023 – Discussion started: 8 June 2023
Revised: 1 September 2023 – Accepted: 13 September 2023 – Published: 25 October 2023

**Abstract.** A measurement campaign was conducted in the Paris region, focusing on the evolution of chemical composition of wet deposition during rainfall events from sequential sampling. A total of eight rain events were documented and characterized by varying meteorological conditions, atmospheric dynamics, and aerosol particle concentrations representative of urban conditions and influenced by long-range mineral dust transport. The intra-event evolution of the chemical composition of wet deposition revealed the predominant role of meteorological parameters and local sources in the observed mass concentration variability. From selected case studies, the washout ratios (WRs) and scavenging coefficients were quantified by conducting simultaneous measurements of aerosol particle composition and wet deposition. The results highlighted a variability of the WR and scavenging coefficients depending on the rainfall rate and on the chemical species. Scavenging coefficients estimated from WR ranged from $5.4 \times 10^{-8}$ to $1.1 \times 10^{-5}\,s^{-1}$ for chemical elements, and they are within the range of values reported in the literature for 0.2–2 µm particle diameters. Our results pointed out that the scavenging coefficient increases with rainfall rate according to a power law, as previously shown in the literature, indicating a stronger removal of particles from the atmosphere with greater precipitation intensity. Quantitative analysis of the data allowed us to estimate the relative contributions of in-cloud scavenging (ICS) for selected rain events. The ICS relative contributions ranged on average from 23 % to 62 % depending on the rain events, and they varied according to the chemical species within the same rain event. This highlights the variability and complexity of the wet deposition process and the influence of specific factors on the contribution of ICS, such as aerosol particle size and hygroscopicity. Overall, this study highlights the variability of wet deposition and its chemical composition and the need to consider the specificities of each event to fully understand the underlying mechanisms.

## 1 Introduction

Wet deposition involves two distinct mechanisms: in-cloud scavenging (hereafter referred to as ICS) and below-cloud scavenging (hereafter referred to as BCS). ICS refers to the scavenging of aerosols within the cloud, where they either act as condensation (or ice) nuclei or are captured by already formed droplets (Seinfeld and Pandis, 2016). BCS is the result of particles being captured through collision by raindrops as they fall (Slinn, 1977). Through these two mechanisms, wet deposition includes locally emitted aerosols that can be scavenged from the atmosphere, and long-range transported aerosols that can be removed by precipitating cloud systems (e.g. Bertrand et al., 2008).

The proportion of ICS and BCS in wet deposition is influenced by a number of factors, including the local environment (e.g. rural or urban) and associated emissions; meteorological variables such as rainfall amount, intensity, and type; and aerosol contents in the atmosphere such as its loading, its size, and its vertical distributions (Aikawa et al., 2014; Ge et al., 2016; Lim et al., 1991; Bertrand et al., 2008; Ge et al., 2021a). The accuracy of the representation of these mechanisms in global and regional modelling is still questionable (Croft et al., 2010), as there are insufficient data to constrain them accurately (Ryu and Min, 2022). Indeed, BCS was considered to be less important than ICS regarding wet deposition in several modelling studies (Croft et al., 2010; Yang et al., 2015; Kim et al., 2021). However, recent observation studies have found that BCS could represent a significant fraction of the wet deposition (Xu et al., 2019; Ge et al., 2021a; Chatterjee et al., 2010; Karşı et al., 2018; Audoux et al., 2023). Grythe et al. (2017) also emphasized the significance of BCS, indicating that it is more responsible for the removal of aerosols in the lower atmosphere, while ICS dominates the wet removal in the free troposphere. These recent findings demonstrate the need to re-evaluate the importance of BCS in regional and global-scale modelling of atmospheric aerosols and thus the necessity to provide more in situ deposition measurements to better constrain them.

Approaches based on only some of the measurable parameters have been used to document the scavenging of atmospheric particles by precipitation. One approach is to compute the washout ratio (also called scavenging ratio and hereafter referred to as WR), which is based on the ratio of the mass or elemental concentrations of wet deposition to those of aerosols measured in the atmosphere (Chamberlain, 1960). WR is a parameter that integrates, without distinction of processes, the relative scavenging efficiency of particulate compounds and chemical elements by considering their transfer from air to water. WR has been regularly used to characterize wet deposition by precipitation for different types of particulate aerosols and chemical compounds found in various atmospheric environments (Jaffrezo et al., 1990; Cerqueira et al., 2010; Marticorena et al., 2017). It can also be used to estimate wet deposition fluxes when given air concentrations and precipitation rates (Duce et al., 1991; Mamun et al., 2022). Moreover, WRs make it possible to study the relative importance of some of the parameters involved in the mechanism of the transfer between the phases, such as rainfall rates (González and Aristizábal, 2012) or aerosol particle size (Jaffrezo and Colin, 1988; Cheng et al., 2021). However, Cheng et al. (2021) have highlighted in their literature review the scarcity of particulate element WR data due to the limited co-located measurements of elements in precipitation and aerosol particles. Another approach is to calculate the scavenging coefficient, which is commonly used in global chemical transport models to represent the below-cloud scavenging of particles by rain (Ge et al., 2021b; Colette et al., 2017). Theoretical studies have primarily focused on determining the particle collection efficiency of raindrops as they fall, while certain numerical, laboratory and field studies have developed semi-empirical parameterizations (Wang et al., 2014; Dépée et al., 2021; Laakso et al., 2003; Slinn, 1977). However, a gap remains between field measurements and theoretical and semi-empirical parameterizations (Wang et al., 2010, 2011). Therefore, the determination of both WR and scavenging coefficient appears to be very useful for future wet deposition studies.

Several studies using sequential sampling have shown a decrease in concentration during the rain event, which is more pronounced in the first few millimetres of rainfall (e.g. Seymour and Stout, 1983; Jaffrezo et al., 1990; Aikawa and Hiraki, 2009). For example, Tanner et al. (2006) found that concentrations measured after 10 mm of rainfall can be 2 to 33 times lower than concentrations measured in the first 2 mm of rainfall, depending on the studied compounds. Sequential rainfall sampling allows for the collection of successive rainfall fractions to monitor the temporal variability of wet deposition (e.g. Laquer, 1990). It is of particular interest to study the dependence of wet deposition content on rainfall characteristics (intensity, droplet size and distribution), which also evolve during the event (Audoux et al., 2023). In addition, the study of the chemical composition of wet deposition and its evolution throughout a rain event allows for determining the influences of several aerosol sources (e.g. anthropogenic or natural). The intra-event evolution of rain chemical composition has also been used to discuss the relative contribution of ICS and BCS mechanisms to wet deposition (e.g. Aikawa and Hiraki, 2009; Ge et al., 2021a; Audoux et al., 2023). Indeed, it is generally assumed that the first increments of the rain event are influenced by both mechanisms, while the last fractions could be attributed to ICS only (Aikawa and Hiraki, 2009; Chatterjee et al., 2010; Germer et al., 2007; Karşı et al., 2018; Desboeufs et al., 2010), although the relative proportion of ICS and BCS evolves during the event (e.g. Zou et al., 2022). Therefore, studying the evolution of wet deposition composition within a rainfall event provides valuable information on the temporal variability and the origin of scavenged aerosol particles, both in terms of sources of pollutant and BCS and ICS mechanisms.

A dedicated sequential precipitation sampler as well as conditioning and chemical analysis protocols were developed to document the intra-event variability of the dissolved and particulate chemical composition of rainfall (Audoux et al., 2023). The present study is based on the analysis of sequential rainfall sampling performed in late winter and spring 2022 at a study site in the Paris region, which included eight case studies with contrasting meteorological conditions, atmospheric loadings, and chemical compositions. This study has two objectives: (1) to document the intra-event evolution of ionic and elemental composition of dissolved and particulate phase species in wet deposition for contrasted rain events and (2) to discuss the parameters influencing wet deposition chemistry through the quantification of washout ratios and scavenging coefficients and the estimation of the relative contribution of BCS and ICS mechanisms in the wet deposition.

## 2 Material and methods

### 2.1 Measurement site and sampling strategy of wet deposition and aerosol particles

The sampling site is located at the air quality station operated by the Interuniversity Laboratory of Atmospheric Systems (LISA), which is inside Université Paris-Est Créteil (UPEC) in the south-east of the Paris agglomeration (48.79° N, 2.44 ° E) (Fig. 1). The study site is in close proximity to various sources of pollution including nearby industries as well as an incinerator, highways, railway stations, and construction sites. Between July 2021 and July 2022, daily rainfall depths measured using a Précis-Mécanique rain gauge (model 3070 A) (0.2 mm precision) at the study site ranged from 0.2 to 37.6 mm. Nineteen percent of rainy days presented rainfall depths lower than 0.4 mm, 12 % were between 0.4 and 1 mm, 40 % were between 1 and 5 mm and 13 % were higher than 10 mm. The sampling strategy is to investigate case studies sampled during an intensive measurement campaign during the winter and spring of 2022. During this period, the daily average $PM_{10}$ ($PM_{2.5}$) concentrations were around 17.5 (11.2) $\mu g\,m^{-3}$ with values reaching up to 57.5 (43.0) $\mu g\,m^{-3}$. Wet deposition collection is performed with a sequential sampler specifically developed at the LISA (Fig. 1a). Sampling, conditioning and analysis of rain samples are described in detail in Audoux et al. (2023); thus, it is only briefly reminded here.

The rain is collected using a Teflon pyramid funnel with a collection surface of 1 $m^2$ in combination with a sampling unit. This unit enables the automatic collection of up to 24 consecutive fractions of rain, adjustable from 0.05 to 2.0 mm, to study dissolved and particulate phase of the wet deposition. The sampling is conducted based on volume, and as a result, it is dependent on the rainfall rate. The sequential sampler is able to correctly collect rainfall fractions for low rainfall intensities, as well as for more intense rainfall recorded by the rain gauge and disdrometer, in comparison to standardized measurements (Audoux et al., 2023). The materials that make up the sampler have been chosen to allow for analysis of the ionic and elemental composition of the dissolved and particulate phase at high and low concentration levels (from several milligrams per litre ($mg\,L^{-1}$) to hundreds of nanograms per litre ($ng\,L^{-1}$)). The sampling bottles and materials that came in contact with the samples underwent a thorough washing protocol in a clean-room laboratory with ISO-7 and ISO-5 level controls.

A summer rain event was collected in July 2021 (R1), and a winter rain event were collected in February 2022 (R2) (Audoux et al., 2023). These case studies are completed here with six additional events collected in late winter and spring 2022, between March (R3, R4, R5, R6 and R7 rain events) and April (R8 rain event). For the 8 rain events studied, between 11 and 32 consecutive fractions have been sampled, with the latter being collected within 10 s to 2 h, depending on the rainfall rate.

Concomitant measurements on atmospheric aerosols and meteorological parameters during the rain sampling are important for a more in-depth understanding of wet deposition mechanisms. Therefore, $PM_{2.5}$ and $PM_{10}$ aerosol mass concentration, as well as the particle size distribution (PSD) between 0.18 and 18 µm, were measured using FIDAS (Fig. 1d), equipped with a TSP Sigma-2 inlet, with a 1 min time step. The FIDAS is an instrument used for regulatory air quality measurement of $PM_{2.5}$ and $PM_{10}$ mass concentration (LCSQA, 2021). Moreover, $PM_{10}$ aerosol particles are sampled on polycarbonate membranes (Nuclepore®, 0.4 µm porosity) using a $PM_{10}$ head sampling (Fig. 1c). Air sampling is done between 15 and 24 h before the start of the rain and is stopped at the beginning of the rain event, within 1 min after removing the cover from the sequential sampler, while the first fraction is being collected. This allows for characterizing the chemical composition of the atmospheric aerosol prior to rainfall. Rainfall rate and droplet size distribution (DSD) are measured using an OTT PARSIVEL® (PARticle SIze and VELocity, Fig. 1e, the Supplement Fig. S1) optical disdrometer with a time resolution of 30 s. In parallel, wind direction and wind speed as well as air temperature and relative humidity are measured using instrumentation from Campbell Scientific© and are recorded with a time step of 1 min. The cloud base height and homogeneity of the atmospheric column are measured using a ceilometer (Vaisala CL31, Fig. 1b and S2). PARSIVEL disdrometers and ceilometers are typically used in multiple measurement networks for precipitation and cloud base height characterization (e.g. Haeffelin et al., 2005; Tapiador et al., 2010). FIDAS, ceilometer and disdrometer measurements are made continuously at the study site, while aerosol filter sampling and deposition measurements are made on alert before or during rain events. This makes it necessary to regularly follow-up the precipitation alerts.

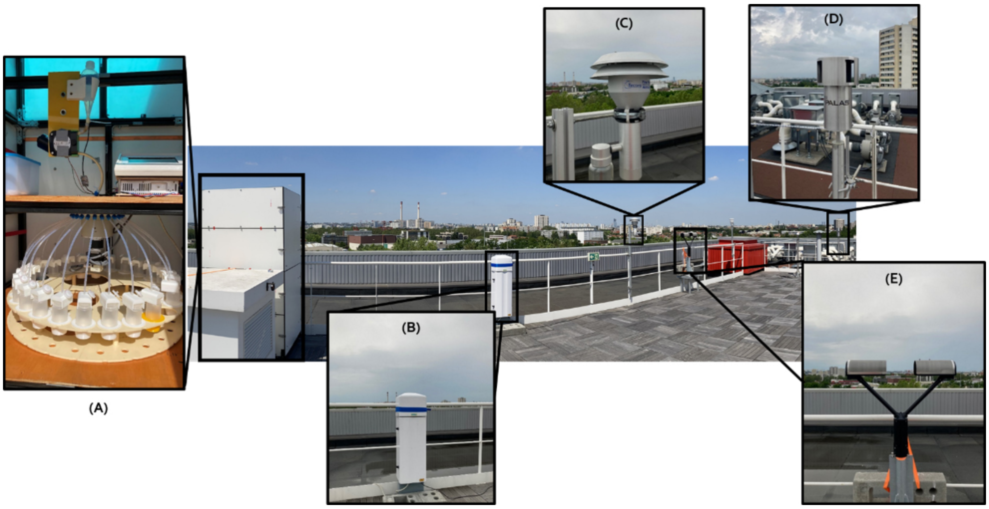


**Figure 1.** Study site. **(a)** Rain sequential sampler; **(b)** ceilometer; **(c)** $PM_{10}$ inlet for filter sampling; **(d)** FIDAS; **(e)** disdrometer.

## 2.2 Elemental and ionic composition analysis of wet deposition and atmospheric aerosol

After sampling, rain samples are quickly processed for ionic and elemental analysis, usually within a time frame of 1 to 12 h after the end of rainfall. If immediate processing is not feasible, the samples are kept in a cool and dark environment at 6 °C and are processed within 24 to 48 h. Treatment, filtration and conditioning are done in a clean-room laboratory with ISO-6 level controls, under a laminar-flow hood (U15 filter), which is estimated to be equivalent to ISO 3. A pH meter (Mettler Toledo Seven2Go) is used to measure the pH of each sequential sample. Samples are then filtered through pre-cleaned Nuclepore® polycarbonate membranes with a porosity of 0.2 µm to separate the particulate phase from the dissolved phase. Following Audoux et al. (2023), the dissolved phase is then divided into two fractions. The first fraction (10 mL aliquot) is frozen until the analysis of water-soluble major inorganic cations ($Na^+$, $NH_4^+$, $K^+$, $Mg^{2+}$, $Ca^{2+}$), anions ($Cl^-$, $NO_3^-$, $PO_4^{3-}$, $SO_4^{2-}$) and organic ions ($HCOO^-$, $CH_3COO^-$, $C_2H_5COO^-$, $CH_4O_3S$, $C_2O_4^{2-}$) by ion chromatography (Compact IC Flex, Metrohm®, PRAMMICS platform). The second fraction (two 15 mL aliquots) is acidified to pH = 1 with nitric acid (Suprapur®) and stored at 6 °C until analysis of water-soluble Al, Ba, Ca, Cr, Fe, K, Mg, Mn, Na, Ni, P, S, Si, Ti and Zn by an inductively coupled plasma atomic emission spectrometer (ICP-AES, Spectro ARCOS Ametek®). The membranes are dried under a laminar-flow hood and conditioned for 48 h at a constant relative humidity of 45 %–50 % and at $T = 20$ °C prior to weighing using a precision microbalance (Mettler Toledo® XPR26C, PRAMMICS platform). In order to accumulate a sufficient amount of material for analysis, several rain sequential samples can be filtered through the same filter. Conversely, when the particulate load is too high, rain fractions can be filtered through multiple membranes. Elemental composition (Al, Ba, Ca, Cr, Fe, K, Mg, Mn, Na, Ni, P, S, Si, Ti and Zn) of the particulate phase is determined using X-ray fluorescence spectrometer (XRF, ZETIUM 4 kW, Malvern Panalytical, PRAMMICS platform). The 0.4 µm porosity Nuclepore® membranes are also analysed using XRF to characterize the elemental composition of the aerosol in the air prior to rainfall events. Our strategy is to monitor the elemental inorganic fraction of the aerosol in order to link it to the rainfall composition. This therefore allows us to characterize about 40 % of the average aerosol composition in the Paris region (Airparif, 2021).

## 2.3 Origin of scavenged aerosol particles

The origin of scavenged aerosol particles can be discussed in relation to their chemical compositions and the trajectory of the air masses. We calculated enrichment factors (EFs; Taylor and McLennan, 1985) in order to determine the origin of elements found in the rain samples. Al is used as the reference for the Earth's crust (hereafter referred to as $EF_X^{crust}$), and Na is used as the reference for sea salt (hereafter referred to as $EF_X^{sea\,salt}$). Equation (1) is used to calculate EF as follows:

$$EF_X(\%) = \frac{([X]/[\mathrm{ref}])_{\mathrm{rain}}}{([X]/[\mathrm{ref}])_{\mathrm{crust\,or\,sea\,salt}}} \times 100, \quad (1)$$

where $([X]/[\mathrm{ref}])_{\mathrm{rain}}$ correspond to the ratio between the element $X$ and the reference (Al or Na) concentrations in rainwater samples and $([X]/[\mathrm{ref}])_{\mathrm{crust\,or\,sea\,salt}}$ the concentrations in the continental crust or in the sea.

To complement local wind measurements at the study site, air mass trajectories were calculated using the HYSPLIT model (https://ready.arl.noaa.gov/HYSPLIT.php) (Draxler and Rolph, 2012). HYSPLIT is a retro-trajectory analysis used to study local-to-continental air mass dispersion and transport of atmospheric compounds (Celle-Jeanton et al., 2009; Bertrand et al., 2008; Calvo et al., 2012) and to determine the origin of air masses to identify sources of atmospheric substances, e.g. mineral-dust, sea salt or anthropogenic sources (Vincent et al., 2016; Anil et al., 2017). Here, 48 or 120 h, depending on the event, backward trajectories were computed by the HYSPLIT model with the Global Forecast System (GFS) (0.25°, global) from the study site (47.79° N, 2.44° W) at the surface (0 m a.g.l.) and at the cloud base height measured by the ceilometer.

## 2.4 Determination of washout ratios, scavenging coefficient and scavenging mechanism contributions

### 2.4.1 Washout ratios

The washout ratio is a parameter used to quantify the relative scavenging efficiency of particulate chemical elements by rain. It is based on the principle of a transfer of the compounds from the air to the water. Therefore, below-cloud WRs are determined from the ratio of the elemental concentration measured in the wet deposition ($C_{\mathrm{rain}}$) to those measured in the air ($C_{\mathrm{air}}$) (Eq. 2).

$$\mathrm{WR} = \frac{C_{\mathrm{rain}}\left(\mu\mathrm{g\,kg^{-1}}\right)}{C_{\mathrm{air}}\left(\mu\mathrm{g\,m^{-3}}\right)} \times \rho_{\mathrm{air}}\left(\mathrm{kg\,m^{-3}}\right) \quad (2)$$

Here, instead of using the whole event for calculation of the WR (Eq. 2) as in the literature (e.g. Cheng et al., 2021), the sequential sampling enables us to use the concentration measured in the first fraction of the rainfall, i.e., the one mainly controlled by the BCS. That is more relevant regarding aerosol scavenging and determination of below-cloud WRs, since this allows us to avoid being affected by the dilution effect reported in the literature (e.g. Jaffrezo et al., 1990).

In order to discuss the relationship between aerosol and wet deposition, information is needed on both aerosol and rain, which we have for R2, R3, R5 and R8. To accurately calculate the WR, it is important to consider the homogeneity of the atmospheric column to ensure the representativeness of surface aerosol measurements. In our study, we observed the presence of a high-altitude aerosol layer using ceilometer measurements (Fig. S2). The atmospheric transport of mineral dust at high altitudes rendered the collected aerosol sample unrepresentative of the scavenged air column. As a result, we excluded the R5 study case from the WR calculation. Therefore, we will focus our discussion on the WR of the element only for R2, R3 and R8.

### 2.4.2 Scavenging coefficient

We can determine the scavenging coefficient ($\Lambda$, $\mathrm{s^{-1}}$) of elements using field measurements and based on the estimation of their washout ratios, as previously done in the literature for sulfate, nitrate and ammonium (Okita et al., 1996; Xu et al., 2019; Andronache, 2004; Yamagata et al., 2009). Indeed, by assuming a uniformly mixed atmospheric column below the cloud base, the average scavenging coefficient of elements can be expressed using Eq. (3), with $R$ and $H$ being the rainfall rate (in $\mathrm{mm\,s^{-1}}$) and the average cloud base height (in m) during the first fraction of rainfall, respectively.

$$\Lambda(\mathrm{s^{-1}}) = \mathrm{WR} \times \frac{R}{H} \quad (3)$$

### 2.4.3 In-cloud vs. below-cloud scavenging

The relative contribution of the ICS mechanism to the measured wet deposition is determined by analysing the mass concentrations of chemical species measured at the end of rainfall (referred to as $C_{\mathrm{ICS}}$). Indeed, due to the scavenging during the initial stages of rainfall, the end of rainfall is characterized by lower PM concentration, which makes the BCS mechanism negligible in terms of wet deposition (e.g. Aikawa and Hiraki, 2009) since the rain composition can be considered representative of the concentrations of droplets in the cloud. Different approaches are used to determine $C_{\mathrm{ICS}}$, such as measuring after a certain amount of rainfall (e.g. 5 mm; Aikawa and Hiraki, 2009; Xu et al., 2017) or selecting the lowest values during rainfall events (Karşı et al., 2018; Berberler et al., 2022). Some authors also fit an exponential decay law and use the constant value as $C_{\mathrm{ICS}}$ (Ge et al., 2021a), while others determine $C_{\mathrm{ICS}}$ using the average value obtained during periods of lower mass concentration variations (Chatterjee et al., 2010). In our case, we selected rainfall events for which the measurements indicated an effective scavenging of the atmospheric column, with a predominant relative contribution of ICS at the end of the event. To select these events, we used the following criteria: (1) the decrease in concentrations measured in the wet deposition, reflecting the evolution of the contribution of the BCS; (2) the decrease in atmospheric concentrations measured using the FIDAS, suggesting a progressive scavenging of the air column under the cloud; and (3) constant concentrations of wet deposition at the end of the event, indicating a steady state between ICS and BCS. From these criteria, the relative contributions of the scavenging mechanisms could be discussed for R1, R2, R4 and R8 case studies.

We determine $C_{\mathrm{ICS}}$, using the volume-weighted mean (VWM) of the last fraction of rain, once a steady state is reached at the end of the rainfall for R1 (1.48–2.65 mm), R2 (1.02–1.33 mm for sulfate, nitrate and ammonium (SNA) and 0.89–1.33 mm for other elements), R4 (2.21–4.42 mm) and R8 (1.87–6.94 mm). The wet deposition flux due to the ICS mechanism can thus be calculated using $C_{\mathrm{ICS}}$ and $P_{\mathrm{tot}}$, the total rainfall depth of the rainfall (Eq. 4) as done previously in the literature (Xu et al., 2017; Aikawa et al., 2014; Ge et al., 2021a).

$$F_{\mathrm{ICS}} = C_{\mathrm{ICS}} \times P_{\mathrm{tot}} \quad (4)$$

Then, the wet deposition flux due to the BCS mechanism ($F_{BCS}$) is determined by subtracting $F_{ICS}$ from the total (dissolved plus particulate) wet deposition ($F_{total}$). Relative contributions of BCS ($BCS_C$) and ICS ($ICS_C$) to wet deposition can be obtained using Eqs. (5) and (6), respectively.

$$BCS_C = \frac{F_{BCS}}{F_{total}}, \tag{5}$$

$$ICS_C = \frac{F_{ICS}}{F_{total}}. \tag{6}$$

## 3 Results

### 3.1 Description of wet deposition case studies

Eight rainfall events constitute a data set illustrating various cases in terms of aerosol concentrations and compositions as well as precipitation properties. The properties of the eight rainfall events studied are listed in Table 1. The rainfall events are characterized by variable rainfall depths ranging from 0.9 to 6.9 mm and mean rainfall rate from 0.4 to 11.5 mm h$^{-1}$. Depending on the rainfall depths and rates, the sampling resolution was adapted. For example, R7 was collected in 22 fractions of volumes ranging from 80 to 440 mL for a rainfall depth of 3.04 mm over 30 min, while R8 was collected in 32 fractions of volumes ranging from 60 to 820 mL for a rainfall depth of 6.9 mm and lasted several hours. Note that for R7 the sampling setup allowed us to only collect the first 3.04 mm of rain of the total event (10.3 mm). Our data set consists of one (12.5 %) event with a rainfall depth of less than 1 mm, one (12.5 %) with a rainfall depth of more than 5 mm, and six others (75 %) representing rainfall depths between 1 and 5 mm. Rain events have varying cloud base heights (from 200 m for R6 up to 2000 m for R8) which, however, can fluctuate within the same event as it is the case for R8.

According to the HYSPLIT 48 h backward trajectory calculation, the origin of the air masses scavenged at the study site remained constant during the duration of the rain events, except for R6 and R8 (Fig. S3). The air masses for R1 and R2 came from the Atlantic Ocean. R3 and R4 had air masses from the Mediterranean at the surface and from Spain and Portugal at the cloud base. For the other events, influenced by mineral dust intrusion from northern Africa, the calculation of HYSPLIT backward trajectories has been performed over 120 h with the same conditions. For R5 and R6, the air masses at the surface came from the United Kingdom via the North Sea and Germany, while the air masses at the cloud base came from northern Africa (south of Tunisia or west of Libya) for R5 and from the Mediterranean Basin and Italy for R6. In the second phase of event R6 (after 09:00 UTC), the air masses at the surface also came from the Mediterranean Basin. For R7, the air masses at the cloud base came from the Mediterranean Basin, and the air masses at the surface came from Libya. For R8, the beginning of the event was characterized by air masses coming from the Atlantic through northern Morocco and Spain at the cloud base and from northern Tunisia at the surface. During the event, the origin of air masses evolved and came from different places in northern Africa (Morocco, Algeria and Tunisia), depending on altitude. This analysis of the backward trajectories shows a close alignment between the origins of these large-scale air masses and the wind directions measured at the surface at the instrumented site in Créteil.

Atmospheric aerosol mass concentrations at the beginning (average over the 30 min prior to the onset of the rainfall) of the R1, R2, R6 and R7 events are primarily controlled by $PM_{2.5}$, which represents 63 %–84 % of $PM_{10}$ concentrations. R3 is characterized by a lower proportion of $PM_{2.5}$, which represents 38 % of $PM_{10}$, while $PM_{2.5}$ measured for R4, R5 and R8 correspond to 46 %–53 % of $PM_{10}$. R1 to R4 took place on days with low particle concentrations, with $PM_{10}$ concentrations lower than of 20 µg m$^{-3}$. During these events, rain had the effect of reducing atmospheric $PM_{10}$ concentrations by 11 %–53 % (Table 1). However, this illustrates the overall effect of the rain event without taking into account the increases in air concentrations that may have been observed during the events (e.g. R8). On the other hand, R5 to R7 occurred on days marked by high concentrations of both $PM_{2.5}$ (33–40 µg m$^{-3}$) and $PM_{10}$ (47–63 µg m$^{-3}$). The latter took place not only during a typical spring pollution episode (Favez et al., 2021), but also during a mineral dust intrusion from northern Africa, as shown by a multi-model dust optical depth simulation provided by the WMO Barcelona Dust Regional Centre (Fig. S4, https://dust.aemet.es, last access: 18 January 2023, Basart et al., 2019). During these events, rain was less effective at reducing $PM_{10}$ concentrations. While R5 is characterized by a decrease in the $PM_{10}$ concentration of the order of 17 %, R6 and R7 show no variation or an increase in the $PM_{10}$ concentration (Table 1). Even though R8 occurred on a day with low particle concentrations, this event was also marked by the intrusion of mineral dust from northern Africa (Fig. S4, Table 1).

Total wet deposition fluxes in our case studies are ranging from 11 to 107 g m$^{-2}$ and are not correlated with rainfall depth nor rainfall rate (Table 1). Indeed, higher wet deposition fluxes are observed for rainfall events (R5 and R6) associated with low rainfall depth but higher pre-rain $PM_{10}$ concentration. However, events characterized by a similar surface $PM_{10}$ mass concentration (R1, R2, R3, R4 and R8) exhibit total wet deposition fluxes that vary over a factor of 4.

The information collected makes it possible to describe eight case studies, illustrating contrasting situations in terms of meteorological conditions, dynamics and atmospheric aerosol loads.

**Table 1.** General information of studied rainfall events.

| Period: date, time (UTC) | Rain no. | Number of rain fractions | Rainfall depth (mm) | Mean rainfall rate ($mm\,h^{-1}$) | Pre-rain $PM_{10}$ concentration ($\mu g\,m^{-3}$) | $PM_{2.5}$ / $PM_{10}$ fraction (%) | After-rain $PM_{10}$ concentration ($\mu g\,m^{-3}$) | Origin of air masses | Cloud base height (m) | Total wet deposition flux ($g\,m^{-2}$) | pH range |
|---|---|---|---|---|---|---|---|---|---|---|---|
| Jun 27 06:55–12:25 | R1 | 21 | 2.65 | 0.48 | 18.7 | 61 | 12.2 | West | – | 11.3 | 5.0–6.0 |
| Feb 10 17:28–20:55 | R2 | 17 | 1.33 | 0.49 | 13.0 | 70 | 6.1 | West | 500–1000 | 12.0 | 6.3–6.8 |
| Mar 11 11:06–13:19 | R3 | 15 | 1.03 | 0.69 | 11.8 | 36 | 9.0 | South-southwest | 2000 | 25.7 | 7.8–7.1 |
| Mar 11 14:16–17:24 | R4 | 17 | 4.42 | 1.41 | 9.9 | 55 | 4.6 | South | 1 200–1500 | 27.8 | 6.0–6.9 |
| Mar 29 13:10–16:50 | R5 | 11 | 0.90 | 0.40 | 62.6 | 52 | 52.1 | North-east (surface) South (cloud base) | 1 500–2000 | 106.3 | 7.8–8.4 |
| Mar 30 04:55–9:31 | R6 | 15 | 1.20 | 0.43 | 44.3 | 82 | 51.7 | South | 200 | 107.1 | 7.2–8.0 |
| Mar 30 15:32–16:01 | R7 | 22 | 3.04 | 11.5 | 47.2 | 80 | 46.6 | South | 1000 | 69.0 | 6.6–7.4 |
| Apr 13 03:00–12:12 | R8 | 32 | 6.94 | 0.90 | 11.9 | 46 | 10.6 | South | 200–2000 | 47.9 | 6.1–7.1 |

## 3.2 Classification of case studies

Volume-weighted mean (VWM) mass concentrations of the particulate and dissolved phases for each rain event are represented in Fig. 2.

Regarding the particulate phase, the average mass concentrations of elements in the rainfall exhibit high variation, with values differing by a factor of 85 between events. The highest concentrations are observed for R5 and R6 events, with 33.9 and 34.5 $mg\,L^{-1}$, respectively. Despite these fluctuations in average mass concentrations, the particulate phase is predominantly composed of Si, Fe and Al, contributing to a relative proportion between 73 % and 85 %. In contrast, the particulate Ca content displays a more pronounced variability, ranging from 3 % to 12 %, depending on the specific rain event.

Regarding the dissolved phase, R4 and R8 are the rainfall events characterized by the lowest dissolved phase VWM concentrations ($\sim 2$ to 3 $mg\,L^{-1}$) and the largest rainfall amounts (4.4 and 6.9 mm for R4 and R8, respectively). These results are consistent with the dependence of wet deposition concentrations with precipitation amount and the dilution effect documented in the literature (e.g. Jaffrezo et al., 1990). The largest concentrations are of the order of 21 $mg\,L^{-1}$ and correspond to the events marked by the mineral dust intrusion from northern Africa but also the lowest precipitation amounts (0.90 mm for R5 and 1.20 mm for R6). The rain events are not characterized by the same contents and relative proportions of acid ($NO_3^-$, $SO_4^{2-}$) or neutralizing ($NH_4^+$) species depending on the rainfall. The dissolved phase is mainly composed of $SO_4^{2-}$, $NO_3^-$ and $NH_4^+$ (SNA), between 58 and 85 % by mass of the analysed species for R1, R2, R3, R4, R7 and R8. In contrast, R5 and R6, and to a lesser extent R8, are composed of a non-negligible proportion of Ca in the dissolved phase (23 %–40 %).

The variations in concentrations of not only acid species but also neutralizing compounds lead to different pH values in the rainfall (Table 1). The progressive scavenging of these compounds during the rainfall event also results in variations in pH (Asman et al., 1982), which is observed between the different events. For instance, R1 has a lower pH (pH $< 5.6$) resulting from lower average concentrations of neutralizing species. Rains R2, R3, R4, R7 and R8 have higher pH values ranging from 6.2 to 6.8 and even basic for R5 and R6 (7.5–8.0). The basic nature of R5 and R6 rains is attributed to the higher Ca contents of mineral dusts present in these rains, which is in agreement with the influence of dust intrusion, as previously described (Ma, 2006; Oduber et al., 2020).

To go further in the interpretation, EFs presented in table 2 as well as origin of air masses (Table 1), are used to classify case studies into three groups: (i) R1 to R4, characterized by air masses from the west and south of France and a significant enrichment in Ca (EF $>$ 15), Ni (EF $>$ 10, except R4), P (EF $>$ 30, except R1), and very high for Zn (EF $>$ 120) and S (EF $>$ 1000); (ii) R5 and R6, characterized by a contribution

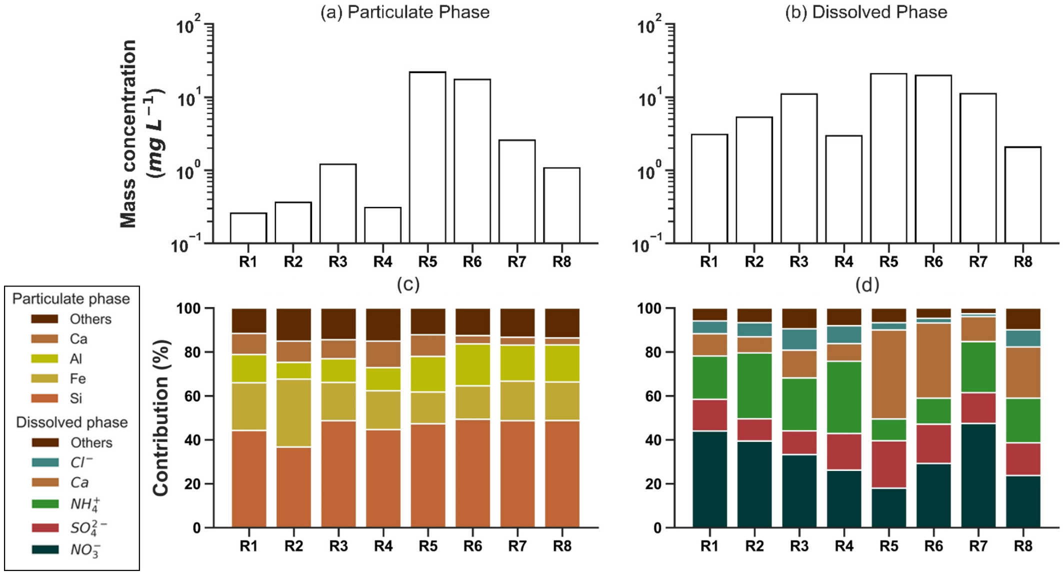


**Figure 2.** Volume-weighted mean mass concentrations ($mg\,L^{-1}$) of **(a)** particulate and **(b)** dissolved phases. Contributions of elements in the elemental composition of particulate phase **(c)** and of chemical species of ionic and elemental composition of dissolved phase **(d)**.

of mineral dust and EFs reflecting mineral sources signature (between 1 and 2), except for Zn (8.0 – 13) and S (119–136), which are still lower than the other rains; and (iii) R7 and R8, characterized by low EFs ($< 10$) for all elements, but higher than R5 and R6 ones, except for Zn (26–44) and S (175–438).

The chemical signature allows us to classify rain events into three categories: R1, R2, R3, and R4 show a marked anthropogenic signature and are hereafter referred to as "anthropogenic" events; R5 and R6 illustrate a distinct mineral dust signature and are hereafter referred to as "mineral-dust" events; and R7 and R8 correspond to mixing conditions and are hereafter referred to as "mixed" events. However, for a given element, the EFs show that the origin is sufficiently homogeneous regardless of the rain events, limiting the data analysis as a function of aerosol sources.

## 4 Discussion

### 4.1 Sequential wet deposition composition

#### 4.1.1 Overall decrease in mass concentration

We firstly quantify for each event an overall decrease in mass concentrations of the particulate (up to a factor of 50) and dissolved (up to a factor of 35) phases, without distinction of the chemical composition (Fig. S5). The decrease factors (DFs) is computed for each rain as the ratio of the mass concentration of the first fraction to the last fraction of rainfall. DFs were 1.4 (R8) to 7.3 (R2) times higher for the particulate phase than for the dissolved phase, depending on the event. This is consistent with a more efficient scavenging of coarse particles (Al, Fe and Si), constituting a significant share of the particulate mass concentration (Fig. 2) compared to the secondary submicron aerosols (SNA) that make up a large proportion of the dissolved phase (Fig. 2), as previously observed in the literature.

Overall, we found that for a given type of rain (anthropogenic in Fig. 3a, b, c, and d; mineral dust in Fig. 3e and f; or mixed in Fig. 3g and h), in other words for atmospheric content of the same order of magnitude and for similar chemical composition (see Table 1 and Fig. 2), the DF increases with rainfall depth (Fig. 3). In addition, R5 and R6 were characterized by high atmospheric aerosol concentrations and a long-range transport of mineral aerosols at high altitude and low rainfall rates ($< 0.5\,mm\,h^{-1}$). The latter explain the low DF, due to high mass concentrations observed throughout the event due to both the low decrease in atmospheric content and the additional contribution of dust particles within the clouds. Within a given event, the elemental DF exhibits significant variability depending on the element (Fig. 3), even when elements share a similar predominant phase and similar size characteristics. For example, in the case of the R4 event, the DF of Cl is 2 times higher than S, while they are predominantly in the dissolved phase, and the DF of Ti is almost 4 times higher than Cr, while they are predominantly in the particulate phase. These observations underline the importance of considering individual element behaviours when assessing wet deposition dynamics.

#### 4.1.2 Intra-event evolution

Sequential sampling enabled the observation of various patterns of concentration evolution during rainfall events. Some events were characterized by a continuous decrease in mass concentrations throughout the rainfall, ultimately reaching a

**Table 2.** Enrichment factors ($EF^{crust}$) of elements measured in the rain events relative to the upper continental crust. Bold values indicate significant enrichment of the element ($EF^{crust} > 10$).

| $EF^{crust}$ | Ba | Ca | Cr | Fe | K | Mg | Mn | Na | Ni | P | S | Sr | Ti | V | Zn |
|---|---|---|---|---|---|---|---|---|---|---|---|---|---|---|---|
| R1 | 7.9 | **19** | 5.6 | 2.5 | 3.2 | 1.4 | 3.8 | 4.8 | **17** | 8.1 | **1 281** | 5.4 | 1.7 | 2.6 | **226** |
| R2 | **20** | **31** | **16** | 6.3 | **12.7** | 1.0 | **9.3** | **16** | **52** | **53** | **1 853** | **9.9** | 4.2 | **16** | **396** |
| R3 | 6.6 | **25** | 5.2 | 2.6 | 5.9 | 1.8 | 5.4 | **13** | **11** | **33** | **1060** | 6.3 | 3.0 | 5.0 | **121** |
| R4 | 7.5 | **17** | 5.6 | 2.7 | 7.0 | 1.5 | 5.2 | 9.9 | 5.4 | **38** | **1521** | 5.2 | 3.0 | **14** | **190** |
| R5 | 2.6 | 6.6 | 2.3 | 1.4 | 1.2 | 1.0 | 1.5 | 0.37 | 0.9 | 3.8 | **136** | 2.8 | 1.7 | 3.1 | **13** |
| R6 | 2.1 | 4.4 | 1.8 | 1.3 | 1.1 | 0.92 | 1.2 | 0.25 | 2.2 | 1.4 | **119** | 2.0 | 1.5 | 2.6 | 8.0 |
| R7 | 4.2 | 7.1 | 4.1 | 1.8 | 1.6 | 1.1 | 1.9 | 0.53 | 3.7 | 4.1 | **438** | 2.7 | 1.8 | 3.1 | **44** |
| R8 | 3.2 | 6.2 | 2.9 | 1.7 | 1.7 | 1.1 | 1.8 | 1.6 | 5.1 | 3.2 | **176** | 2.1 | 1.8 | 3.3 | **26** |

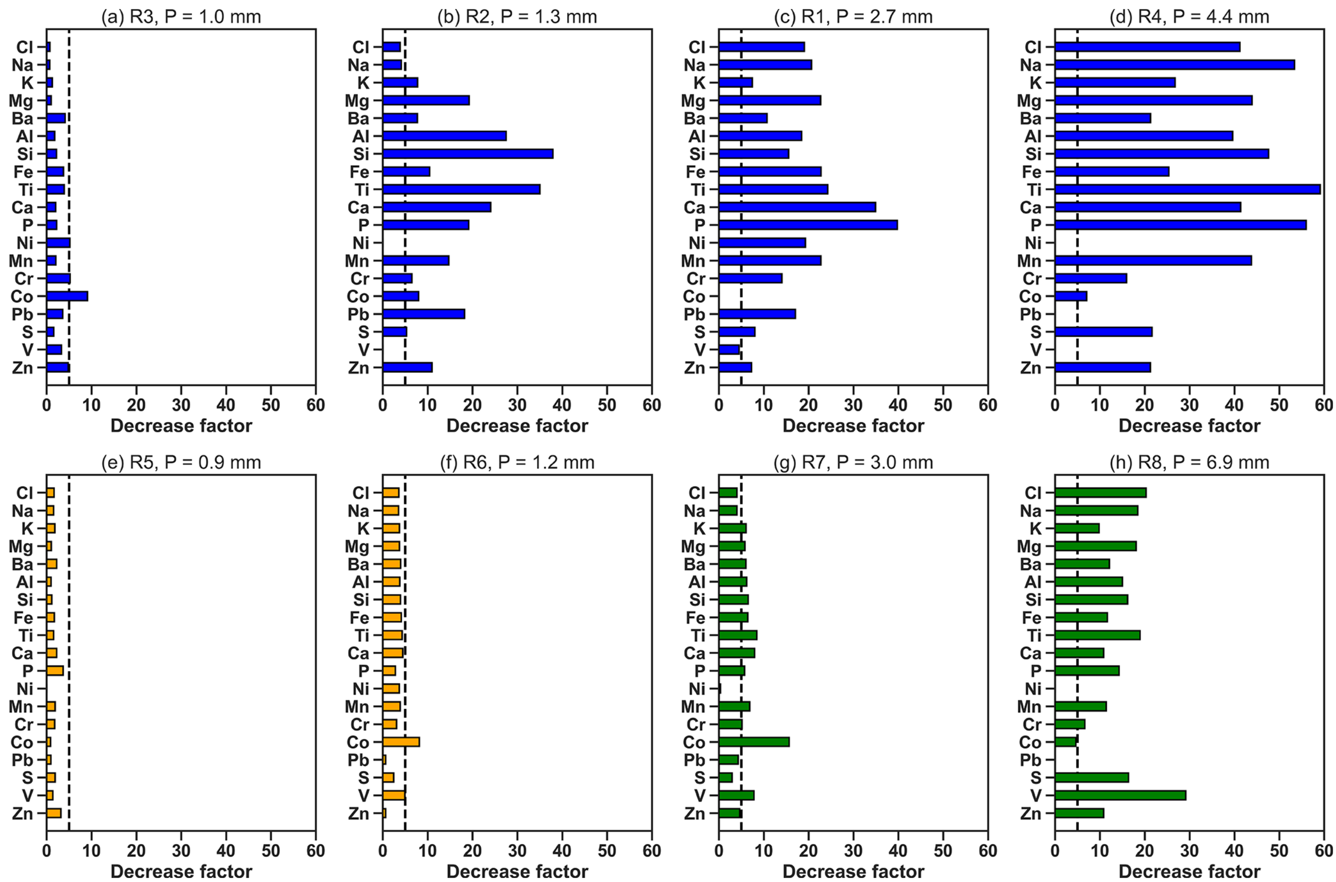


**Figure 3.** Element decrease factor (DF) for each rain event. The dotted line marks DF = 5. A missing bar means that the concentration in the first fraction and/or the last fraction of rainfall is below the detection limit. Blue bars, orange bars, and green bars correspond to anthropogenic, mineral dust, and mixed events, respectively.

lower and constant level in the final fractions regardless of the phase or the chemical species (R1, R7). This kind of evolution is commonly found in the literature, with a high-decreasing trend in the first 1 to 3 mm, until reaching a constant level until the end of the rainfall, for both dissolved and particulate phases (e.g. Jaffrezo et al., 1990; Kasahara et al., 1996). In contrast, although lower and constant levels were reached at the end of rainfall, R4, R5 and R8 exhibited punctual increases or stabilization of the concentrations of both phases during the rainfall, while R2, R3 and R6 events showed only punctual increases in the dissolved phase.

As an illustration, Fig. 4 shows the temporal evolution of atmospheric concentrations ($PM_{10}$ and $PM_{2.5}$), the evolution of mass concentrations of dissolved and particulate phases, and rainfall intensity and droplet concentrations (i.e. the number of droplets measured by the disdrometer divided by the unit of volume of the collected rain fraction) during the R6 and R8 events. It has been observed that atmospheric concentrations evolve differently according to particle size classes ($PM_{2.5}$ vs. $PM_{2.5–10}$) and rainfall phases. Generally, precipitation is associated with a decrease in atmospheric concentrations during rainfall (Table 1), except for event R6 (Fig. 4f). However, an increase in concentrations of the coarse aerosol fractions ($PM_{2.5–10}$) is observed quite systematically as rainfall intensities decrease below 0.5 $mm\,h^{-1}$, especially for events R2, R4 and R8 (between 04:00 and 05:00) as shown in Fig. 4a.

An increase in wet deposition concentrations during rainfall has been previously observed by some authors (e.g. Karşı et al., 2018). Here, the latter were systematically correlated with a decrease in precipitation intensity (Fig. 4d, i) and an increase in droplet concentration (Fig. 4e, j). Several possible explanations are considered for these observations: this could be due to either an effect of "over-concentration" of falling raindrops or a release of aerosols due to their evaporation (Huff and Stout, 1964; Baechmann et al., 1996a, b; Gong et al., 2011); alternatively, it could be due to an increase in scavenging efficiency due to the reduction of droplet size distribution, implying a larger effective surface of capture (e.g. Jones et al., 2022) as well as to a local emission phenomenon (Karşı et al., 2018).

The high temporal resolution of the sampling and, hence, the determination of the chemical composition of the dissolved and particulate phases, allows for identifying more accurately the cause of these concentration increases.

For rainfall events R4 and R8 (Fig. 4a–e), notable increases in concentration during the rain are observed for both the particulate and dissolved phases. These increases appear to be associated with higher precipitation in altitudes compared to the surface, as indicated by the ceilometer measurements. A plausible explanation for these observations could be the partial evaporation of raindrops as they fall, leading to a reduction in their diameter and a subsequent increase in mass concentration. It is assumed that only water evaporates in this process, while the chemical species contained in the raindrops remain. Consequently, the initial material removed by the droplets, expressed in terms of their volume, becomes greater (Baechmann et al., 1996b). On the contrary, if the evaporation of the droplets is complete as they fall, this can result in the release of aerosols into the atmosphere, thereby increasing atmospheric concentrations (Huff and Stout, 1964; Gong et al., 2011). This release can then affect the mass concentrations of subsequent raindrops, as falling raindrops capture the released aerosols.

For R6, there is also an increase in mass concentrations during rainfall, but only for some species (Fig. 4f–j). $NO_3^-$ and $NH_4^+$ concentrations increase by a factor of 4 to 5, while dissolved Zn and Cu concentrations increase by a factor of 5 to 16 (included in the "others" category in Fig. 2). The observed increase in $NO_3^-$ and $NH_4^+$ mass concentrations in precipitation may be attributed to an additional input by local emissions. During this period, between 07:00 and 09:00 UTC, low precipitation rates and a very low boundary layer height are observed, with the cloud base height around 200 m. This specific time frame corresponds to a period of significant road traffic, which is in proximity to the monitoring site. In addition, the $NO_x$ concentrations measured at the LISA air quality station during the same time steps also display increases of more than a factor of 5. Considering that $NO_x$, Zn and Cu are tracers of automotive activity (Thorpe and Harrison, 2008; Bukowiecki et al., 2009; Pant and Harrison, 2013), this observation provides further support for the hypothesis of the influence of local emissions (in this case road traffic) on the increase in mass concentrations of wet deposition throughout the event. R6 is therefore a good case study to illustrate the combined influence of changing meteorological parameters and local sources on the evolution of deposition concentrations during a rain event.

By conducting a comprehensive analysis of precipitation characteristics, atmospheric dynamics and local influences, we aimed to shed light on the underlying mechanisms responsible for the observed punctual increases in mass concentrations during our study cases. Our results highlight the importance of the droplet size distribution, its evolution and the presence of local sources that also evolve during the rain event. Such investigations are essential to unravel the complexities of wet deposition dynamics and deepen our understanding of the intricate interactions between atmospheric particles and wet deposition processes.

### 4.2 Washout ratios and scavenging coefficient

The developed measurement strategy for both the chemical characterization of aerosol and wet deposition (see Sect. 2.3) enables us to compare the concentrations in the air and in the first samples of rain, excluding the effect of dilution. Total mass concentrations estimated from chemical analysis of aerosol filters represent from 15 % (R3) to 55 % (R8) of the measured $PM_{10}$ mass concentration (Table 1), depending on the situations.

Total mass concentrations measured in the first fraction of rainfall events (0.06 to 0.10 mm) are higher when pre-rain $PM_{10}$ surface concentrations are greater (Table 1). However, for R2, R3 and R8, $PM_{10}$ concentrations are of the same order of magnitude (11.8–13 $\mu g\,m^{-3}$), while total mass concentrations in their first fraction differ by a factor 1.8 (R2: 28.1 $mg\,L^{-1}$; R3: 49.8 $mg\,L^{-1}$; R8: 38.7 $mg\,L^{-1}$). The latter is higher when the $PM_{2.5}$ / $PM_{10}$ ratio is lower (Table 1). This suggests that $PM_{2.5}$ values are scavenged less effectively than coarser particles ($PM_{2.5–10}$). R6 and R7 events are characterized by similar pre-rain $PM_{10}$ surface concentrations as well as similar $PM_{2.5}$ / $PM_{10}$ ratios. However, the R6 event shows total mass concentrations in the first fraction that are 2.4 times higher than R7 (68.3 $mg\,L^{-1}$). This can be explained by the long-range transport of mineral dust at high altitude. Therefore, wet deposition fluxes at the be-

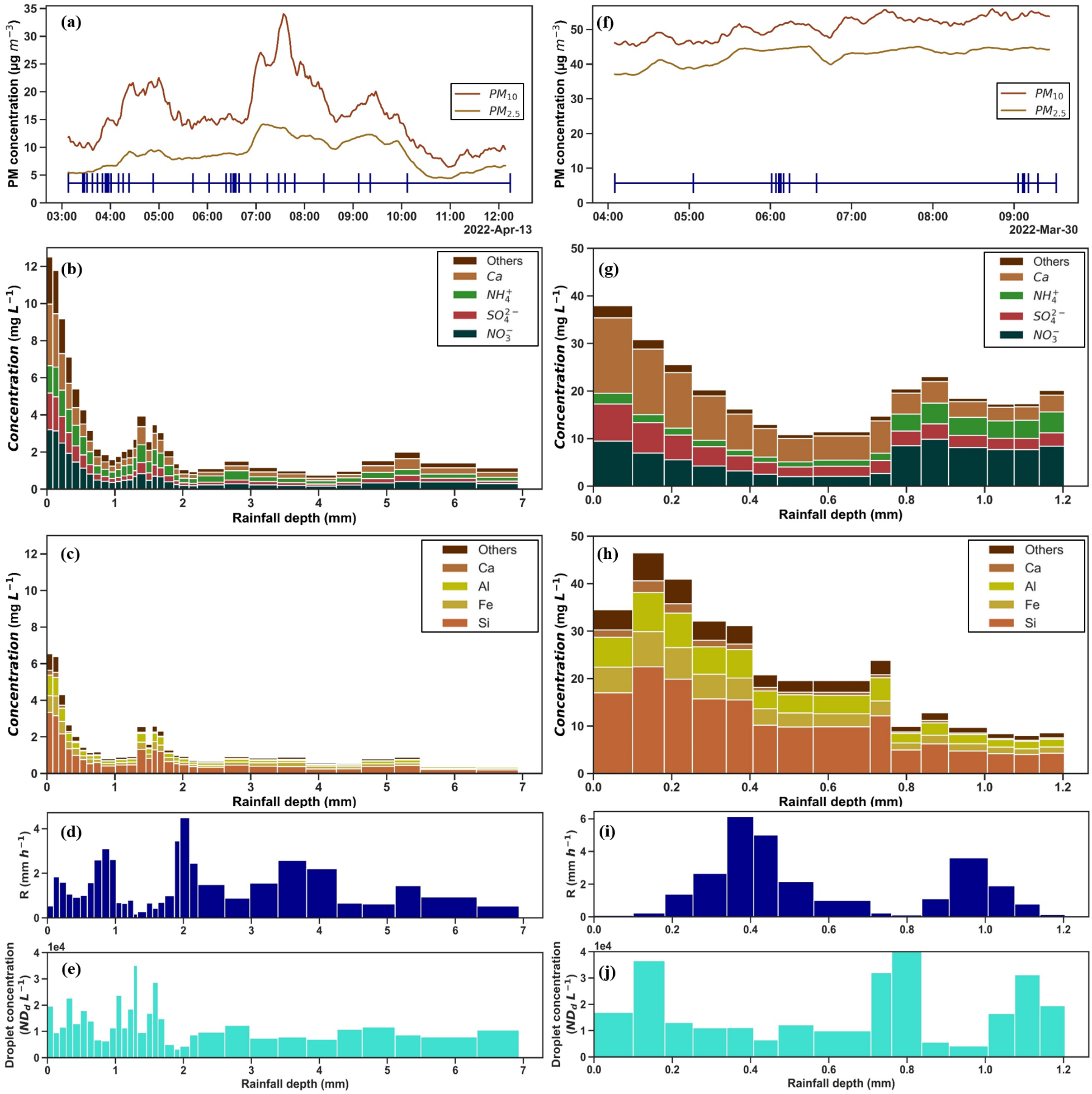


**Figure 4.** R8 **(a–e)** and R6 **(f–j)** case studies. Evolution of $PM_{10}$ and $PM_{2.5}$ concentrations ($\mu g\,m^{-3}$; **a** and **f**) with time. The different sampling periods for each rain fraction are indicated by the intervals in blue **(a, f)**. Evolution of dissolved mass concentration ($mg\,L^{-1}$; **b, g**), particulate mass concentrations ($mg\,L^{-1}$; **c, h**), rainfall intensity ($R$ in $mm\,h^{-1}$; **d, i**) and droplet concentration ($ND_d\,L^{-1}$; **e, j**) throughout rain events.

ginning of rainfall seem to be primarily correlated to $PM_{10}$ surface concentrations and secondly to the coarse fraction ($PM_{2.5\text{–}10}$ / $PM_{10}$). This is consistent with the aerosol size dependence of scavenging mechanisms and the minimal efficiency of the BCS mechanism between 0.2 and 2 μm (e.g. Wang et al., 2010).

Figure 5 depicts the total concentration of elements (dissolved plus particulate) in the first rain fraction ($\mu g\,kg_{rain}^{-1}$) plotted against the total concentration of elements measured in the aerosol ($\mu g\,kg_{air}^{-1}$) for R2, R3 and R8 rain events, i.e. the only rain samplings adapted for this comparison. According to Eq. (2), the ratios in these two concentrations illustrated in Fig. 5 correspond to the WR for analysed species (Table S6

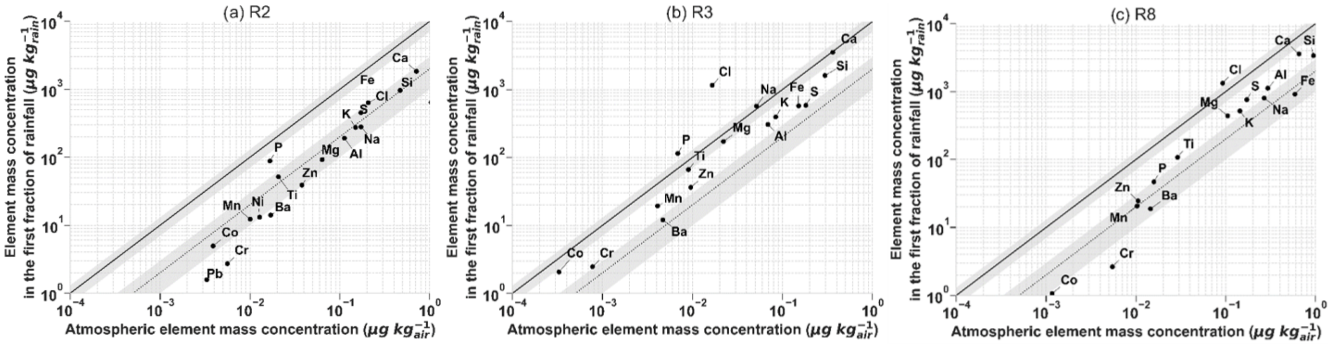

**Figure 5.** Element mass concentration in the first fraction of the rainfall ($\mu g\,kg_{rain}^{-1}$) as a function of the element mass concentration in the aerosol ($\mu g\,kg_{air}^{-1}$) of **(a)** R2, **(b)** R3 and **(c)** R8. The solid lines with envelopes correspond to washout ratios of the order of $10\,000 \pm 3000$, while the dashed lines with envelopes correspond to washout ratios of $2000 \pm 1000$.

in the Supplement). It appears that the scavenging efficiency is clearly dependent on the element. As an example, for similar particulate mass concentrations ($0.02\,\mu g\,kg_{air}^{-1}$), we found higher P concentration in the first fraction of R2 ($88\,\mu g\,kg_{rain}^{-1}$) in comparison to Ba ($14\,\mu g\,kg_{rain}^{-1}$).

We found that for a given rain event, WR values can vary by up to a factor of 11 to 30 from one element to another (Table S6). WRs of elements found in R2 are primarily in the $2000 \pm 1000$ envelopes, while WRs of R3 are systematically higher. Regarding R8 events, we observed an intermediate behaviour in terms of WR values. In all the cases, the WR values are higher than the values previously estimated, in agreement with the dilution effect on the WR values available in the literature. Indeed, by taking into account the first fraction of the rainfall, the calculation minimizes the influence of the ICS contribution as opposed to the WR values considering the entire event. The difference in WR as a function of element could be due to either an additional source of elements in the rain (e.g. ICS or gas phase scavenging); a difference in BCS efficiency, e.g. due to different size distribution or hygroscopicity of the element-bearing particles; or a contribution of PM with a diameter greater than 10 µm (e.g. Jaffrezo and Colin, 1988; Cheng et al., 2021; Kasper-Giebl et al., 1999; Cheng and Zhang, 2017). Cheng et al. (2021) emphasized the predominant role of particle size distribution on the WR. Indeed, the elements associated with the coarse mode ($PM_{2.5-10}$) present the largest WR, except Si and Fe, while the elements that are dominant in the fine particles ($PM_{2.5}$) had a lower WR. Even if we have no information on the size distribution of aerosol chemical composition, the EF shows that the elements associated with a coarse mode by Cheng et al. (2021) are from a dust origin, and those associated with the fine mode (e.g. S, Zn) are of an anthropogenic origin, in our samples. Our results are consistent with these observations: elements linked to coarse particles, such as calcium (WR ranging between 2500 and 9800), exhibit higher WR values compared to those associated with fine particles, such as zinc (WR ranging between 1000 and 3800). However, as highlighted in the review of Cheng et al. (2021), some elements found primarily in the coarse mode, such as Fe (WR = 3800), exhibit similar WR value to elements associated with fine particles (e.g. Zn) as illustrated in event R3.

However, our study revealed a significant variation between different events for the same chemical species. Interestingly, for each element (except S), this variability consistently follows a decreasing trend in WR with increasing pre-rain $PM_{2.5}$ / $PM_{10}$ fraction (Table 1). In addition, we observed an increasing trend in WR with higher rainfall rates. For instance, WR of Ca increase from 2500 to 9800 when rainfall rate increases from 0.5 to $1.2\,mm\,h^{-1}$. This shows that the particle size distribution is probably not the major factor acting on particle below-cloud wet scavenging. These results are particularly noteworthy because they represent the first instance of WR measurements unaffected by the dilution effect.

Scavenging coefficients (i.e. $\Lambda$) can be determined from the WR calculation using Eq. (3). These estimations are the first available for major and trace metals. Figure 6 illustrates $\Lambda$ of elements as a function of rainfall rate. Our results show that $\Lambda$ increases with rainfall rate according to a power law, as previously shown in the literature (e.g. Xu et al., 2019; Wang et al., 2014). At a rainfall rate of $R = 1\,mm\,h^{-1}$, we obtained $\Lambda$ values between 0.5 and $1.3 \times 10^{-6}\,s^{-1}$, with the exception of chlorine. These values fall within the range ($2.6 \times 10^{-7} - 1.7 \times 10^{-6}\,s^{-1}$) documented for radionuclides by Sparmacher et al. (1993) for controlled experiments with similar rainfall rate and aerosol diameters (0.98 and 2.16 µm). Scavenging coefficient evolution with rainfall rate varies from one element to another, with slopes ranging from 0.5 for sulfur to 2.9 for chlorine. These differences cannot be attributed solely to mass concentration, particle size, or water-soluble fraction of elements. For instance, while elements associated with the same aerosol types, such as Na and Cl or Al, Ti, and Si, show similar behaviour with rainfall rate, chlorine and sulfur exhibit contrasting trends

**Table 3.** Relative ICS contribution ($ICS_C$) for R1, R2, R4 and R8 events. Bold values indicate the predominance of ICS.

| Chemical species | $ICS_C$(%) | | | |
|---|---|---|---|---|
| | R1 | R2 | R4 | R8 |
| $SO_4^{2-}$ | **62** | 48 | 23 | **58** |
| $NO_3^-$ | 35 | **55** | 27 | **57** |
| $NH_4^+$ | 45 | 40 | 24 | **65** |
| Al | 44 | 38 | 20 | **62** |
| Ba | 37 | **50** | 26 | **68** |
| Ca | 21 | 35 | 16 | **64** |
| Cl | 36 | **88** | 20 | 49 |
| Cr | 44 | **67** | 30 | **75** |
| Fe | 37 | 48 | 26 | **70** |
| K | **67** | 41 | 26 | **70** |
| Mg | 33 | 33 | 18 | **57** |
| Mn | 36 | 41 | 19 | **71** |
| Na | 32 | **85** | 17 | **53** |
| P | 24 | 30 | 17 | **57** |
| Pb | **82** | 37 | 18 | **71** |
| Si | 48 | 31 | 18 | **61** |
| Sr | 21 | 33 | 15 | **60** |
| Ti | 42 | 29 | 17 | **69** |
| V | 37 | **68** | **59** | 37 |
| Zn | **59** | 33 | 18 | **67** |
| Average ± SD | 42 ± 15 | 47 ± 17 | 23 ± 9 | **62 ± 9** |

even though they are both water-soluble elements. Similarly, scavenging coefficients for coarse particles (e.g. Al and Si; $1.5–8.5 \times 10^{-7}\,s^{-1}$) are comparable to those for fine particle (Zn and S; $0.9–6 \times 10^{-7}\,s^{-1}$). Aerosol scavenging does not depend on a single parameter but is governed by the interaction of several parameters including the intrinsic properties of the aerosol (size,solubility) and of the precipitation (intensity, size and number of droplets). Consequently, our results underline the critical role of rainfall rates and aerosol particle properties for the determination of both WR and $\Lambda$.

## 4.3 Contribution of in-cloud and below-cloud scavenging

The $ICS_C$ of chemical species analysed in the selected rains (see Sect. 2.4) are presented in Table 3. We observe significant variations in $ICS_C$ within individual events for different chemical species, as well as different $ICS_C$ values of the same chemical species between different events.

For R1, R2 and R4 anthropogenic events, the elements of crustal origin found in the coarse fraction of aerosols (Al, Si, Fe, Ti, Ca, Mg, Sr) are mainly deposited via the BCS mechanism. This observation is consistent with previous in situ studies conducted in urban environments, which have reported that the BCS mechanism accounts for a significant proportion (ranging from 52 % to 99 %) of calcium wet deposition (Ge et al., 2016; Karşı et al., 2018; Ge et al., 2021a; Berberler et al., 2022). The wet deposition of Mn and $NH_4^+$ is mainly attributed to the BCS mechanism, accounting for 55 % to 87 %. This corresponds to a similar range of values reported for $NH_4^+$ in other urban environments in Austria (65 %), Türkiye (60 %–95 %) and China (47 %–84 %) (Xu et al., 2017; Karşı et al., 2018; Berberler et al., 2022; Monteiro et al., 2021; Ge et al., 2021a). In the literature, the $BCS_C$ mechanism for sulfate and nitrate in urban environments shows large variations, with reported values ranging from 50 % to 98 % (Ge et al., 2016; Xu et al., 2017; Karşı et al., 2018; Ge et al., 2021a; Monteiro et al., 2021; Berberler et al., 2022) and as low as 16 % for sulfate (Aikawa et al., 2014). In our study, the $BCS_C$ of sulfate and nitrate in anthropogenic events varies between 38 % and 77 %, depending on the events. Few chemical species show a predominance of the ICS mechanism in the wet deposition of anthropogenic events that could possibly be influenced by seasonal factors, different local sources (such as oil and wood heating systems for $SO_4^{2-}$, Zn), gas scavenging contributions (with nitrate being mainly gaseous in summer and particulates in winter) (Audoux et al., 2023), or long-distance transport. For instance, seasonal factor and difference in local sources explain higher $ICS_C$ for $SO_4^{2-}$ and Zn in R1 in comparison to R2 and R4. In addition, the higher $ICS_C$ obtained for Na and Cl for R2 may be linked to the origin of air masses coming from the Atlantic Ocean. Overall, anthropogenic events are, on average, primarily influenced by the BCS mechanism, accounting for 53 % to 77 % of the wet deposition of chemical species.

In contrast, for the mixed event R8, influenced by both local sources and long-distance transport of mineral dust, the majority of chemical species, except for V (37 %) and Cl (49 %), are predominantly deposited through the ICS mechanism, accounting for 57 % to 75 % of their wet deposition. While the long-distance transport of mineral dust may explain the pronounced contribution of the ICS mechanism for some crustal elements, it is evident that this factor alone cannot account for the prevalence of ICS for all chemical species. Certain elements observed in event R8, such as $NH_4^+$, are not associated with mineral dust. Since the rainfall depth is higher in this case, the higher ICS contribution can be due to an effective scavenging of the air column below the cloud (Ge et al., 2021a). Indeed, the wet deposition that occurs after the depletion of the atmospheric column below the cloud is primarily influenced by aerosol transported and scavenged within the cloud, explaining a high contribution of the ICS mechanism.

Several factors may contribute to these differences in the observed contribution of ICS and BCS between events. One key factor is the variation in meteorological conditions, including intensity, droplet size, and cloud base height, as well as $PM_{10}$ concentrations (Table 1). Numerical studies have highlighted the importance of not only cloud height but also cloud thickness in the relative contribution of BCS and ICS (Kim et al., 2021; Migliavacca et al., 2010; Wiegand et al., 2011). This dependence can be explained by the fact that

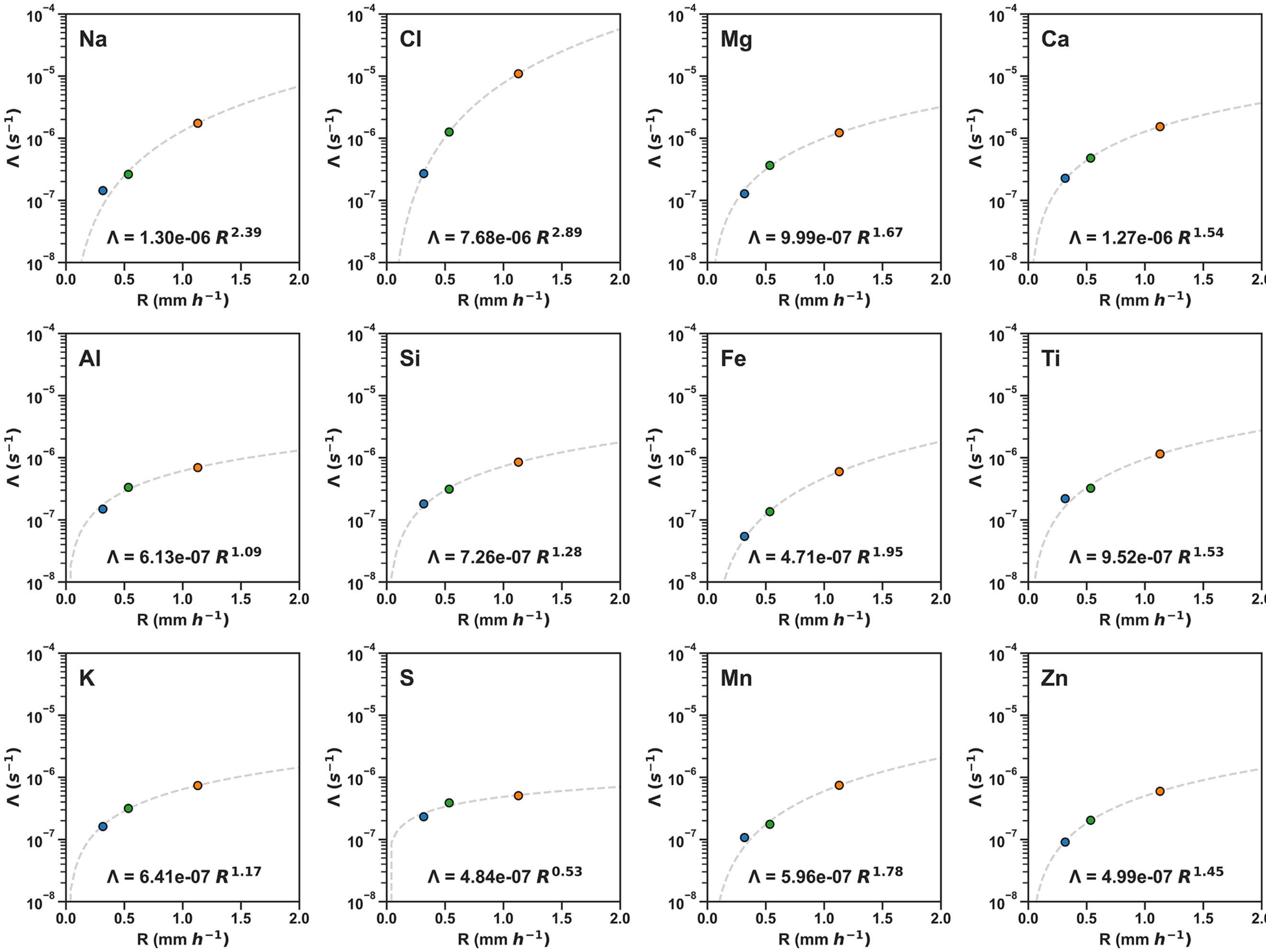


**Figure 6.** Scavenging coefficient ($\Lambda$, $s^{-1}$) as a function of rainfall rate ($R$, $mm\,h^{-1}$) for studied elements. Blue, orange and green dots correspond to events R2, R3 and R8, respectively.

the higher the cloud height, the greater the volume of air swept by the droplets and therefore the greater the quantity of aerosols encountered by the precipitating droplets, at equal and homogeneous concentration on the atmospheric column. For example, event R1 has higher $PM_{10}$ concentrations but 2 to 4 times lower rainfall depth compared to other anthropogenic events. In addition, R4 has a higher cloud base height compared to R2, which could affect the $BCS_C$ despite the higher precipitation amount and lower $PM_{10}$ concentration. These variations in meteorological conditions and atmospheric dynamics could influence BCS efficiency as well as aerosol content to be scavenged below the cloud, leading to the observed discrepancies in $BCS_C$ and $ICS_C$ values. Consequently, the complex interactions between meteorological conditions, aerosol properties, local sources and long-range transport can result in different scavenging behaviours for each event, highlighting the challenge and the need for wet deposition studies.

## 5 Conclusion

A measurement campaign has been performed in the south-east of the Paris agglomeration to monitor the evolution of chemical composition of wet deposition with time during rainfall events. The collected rainfall events illustrate contrasting situations in terms of meteorological conditions (rainfall depth and intensity), atmospheric dynamics (cloud base height between 200 and 2500 m), and different atmospheric $PM_{10}$ concentrations ranging from 10 to more than $60\,\mu g\,m^{-3}$, characterized by the urban environment of the study site but also by mineral dust intrusions from the Sahara. Using additional measurements, three categories of events were identified according to the origin of the aerosols found in the rain: anthropogenic (R1 to R4), mineral-dust (R5 and R6) and mixed rainfall events (R7 and R8).

Our study illustrates the variability of both the mass concentrations and the chemical composition of the particulate and dissolved phases. For the different rains sampled, we observe a rapid decrease in mass concentrations as the rain progresses. The decrease is more pronounced for the particulate fraction (up to a factor of 50) than for the dissolved fraction (up to a factor of 33), regardless of the event. However, some phases of increasing mass concentrations have been identified during certain events. We have proposed several hypotheses, such as local sources, evaporation of droplets and an increase in scavenging efficiency, that warrant the need to thoroughly document the precipitation characteristics, atmospheric dynamics, and surface $PM_{10}$ and $PM_{2.5}$ contents throughout the entire rainfall event.

Initial chemical composition of rainfall and the chemical composition of atmospheric $PM_{10}$ allowed us to calculate washout ratios (WRs) describing the very beginning of the rainfall, before the dilution effect occurs when the contribution of below-cloud scavenging is greater. WR varied from below 2000 for one event to up to 10 000 for another, depending on the chemical species, and was consistent with an increasing trend with increasing rainfall rate. Scavenging coefficients were also determined based on the WR, rainfall intensity and cloud base height. We obtained values in the range of $5.4 \times 10^{-8}$ to $1.1 \times 10^{-5}\,s^{-1}$ for studied elements. We found a power-law increase in the scavenging coefficient with the rainfall rate, as previously shown in the literature, indicating a greater removal of particles from the atmosphere at higher rainfall intensities. However, evolutions are not directly linked to aerosol size or solubility but rather to the multiple intrinsic parameters of aerosol and precipitation. The implications of these results are substantial, as they emphasize the need to consider rainfall characteristics and aerosol properties for accurate estimations of the scavenging process and its impact on atmospheric deposition. Such efforts will help refine and develop more reliable parameterizations that can accurately represent scavenging efficiency for a wider range of environmental conditions.

We estimate the contributions of the in-cloud scavenging (ICS) and below-cloud scavenging (BCS) mechanisms for some rainfall events (R1, R2, R4 and R8). The results show a significant contribution of both mechanisms, with a higher contribution of the BCS mechanism, between 53 % and 77 % in average, for rainfall events characterized by a larger anthropogenic contribution and local sources (R1, R2 and R4). However, the contributions of scavenging mechanisms are as variable from one chemical species to another as they are from one rainfall to another, depending on their specific sources, atmospheric dynamics and meteorological conditions. The mixed event (R8), characterized by long-distance transport of mineral dust, shows a predominant contribution of the ICS mechanism, from 57 % to 75 % depending on the chemical species. It is difficult to determine a general trend based on a limited number of events because of the complex interactions between meteorological conditions, aerosol properties, local sources and long-range transport that can result in different scavenging behaviours for each event. However, our findings provide new directions for future research, particularly regarding the effect of droplet size distribution and the effect of cloud base height on wet deposition dynamics.

To gain a comprehensive understanding of the factors influencing scavenging mechanisms, further investigation is necessary, including a larger data set covering a wider range of meteorological conditions and aerosol characteristics. Such a comprehensive approach will enable a more robust analysis and confirm and/or identify the dominant factors that drive scavenging during rainfall events.

**Data availability.** The dataset used for this study is available for download for research and educational purposes at the following web link: http://www.lisa.u-pec.fr/fr/donnees maintained by Laboratoire Interuniversitaire des Systèmes Atmosphériques (2023).

**Supplement.** The supplement related to this article is available online at: https://doi.org/10.5194/acp-23-13485-2023-supplement.

**Author contributions.** TA: conceptualization, formal analysis, investigation, writing (original draft), writing (review and editing), visualization. BL: conceptualization, investigation, writing (review and editing), supervision, funding acquisition, project administration. KD: formal analysis, investigation, writing (review and editing). FM: methodology, resources. GN: formal analysis, resources. OL: formal analysis. SC: conceptualization, formal analysis, project administration.

**Competing interests.** The contact author has declared that none of the authors has any competing interests.



**Acknowledgements.** Some of the analyses (CI, XRF) presented were performed with the instruments of the PRAMMICS platform OSU-EFLUVE UMS 3563. The authors gratefully thank the two anonymous reviewers for their useful comments and critiques that have contributed to improving the manuscript.

**Financial support.** This work is performed in the framework of the research programmes DATSHA supported by the French national programme LEFE (Les Enveloppes Fluides et Environnement) and Foundation Air Liquide and was also supported by LISA, UPC, UPEC, UMR CNRS 7583 via its internal project call.

**Review statement.** This paper was edited by Armin Sorooshian and reviewed by two anonymous referees.

## References

Aikawa, M. and Hiraki, T.: Washout/rainout contribution in wet deposition estimated by 0.5 mm precipitation sampling/analysis, Atmos. Environ., 43, 4935–4939, https://doi.org/10.1016/j.atmosenv.2009.07.057, 2009.

Aikawa, M., Kajino, M., Hiraki, T., and Mukai, H.: The contribution of site to washout and rainout: Precipitation chemistry based on sample analysis from 0.5 mm precipitation increments and numerical simulation, Atmos. Environ., 95, 165–174, https://doi.org/10.1016/j.atmosenv.2014.06.015, 2014.

Airparif: Synthèse des connaissances sur les particules en Île-de-France, https://www.airparif.asso.fr/sites/default/files/documents/2021-04/Note_particules_042021.pdf (last access: 2 March 2022), 2021.

Andronache, C.: Estimates of sulfate aerosol wet scavenging coefficient for locations in the Eastern United States, Atmos. Environ., 38, 795–804, https://doi.org/10.1016/j.atmosenv.2003.10.035, 2004.

Anil, I., Alagha, O., and Karaca, F.: Effects of transport patterns on chemical composition of sequential rain samples: trajectory clustering and principal component analysis approach, Air Qual. Atmos. Hlth., 10, 1193–1206, https://doi.org/10.1007/s11869-017-0504-x, 2017.

Asman, W. A. H., Jonker, P. J., Slanina, J., and Baard, J. H.: Neutralization of Acid in Precipitation and Some Results of Sequential Rain Sampling, in: Deposition of Atmospheric Pollutants: Proceedings of a Colloquium held at Oberursel/Taunus, West Germany, 9–11 November 1981, edited by: Georgii, H.-W. and Pankrath, J., Springer Netherlands, Dordrecht, 115–123, https://doi.org/10.1007/978-94-009-7864-5_12, 1982.

Audoux, T., Laurent, B., Chevaillier, S., Féron, A., Pangui, E., Maisonneuve, F., Desboeufs, K., Triquet, S., Noyalet, G., Lauret, O., and Huet, F.: Automatic sequential rain sampling to study atmospheric particulate and dissolved wet deposition, Atmos. Environ., 295, 119561, https://doi.org/10.1016/j.atmosenv.2022.119561, 2023.

Baechmann, K., Ebert, P., Haag, I., and Prokop, T.: The chemical content of raindrops as a function of drop radius – I. Field measurements at the cloud base and below the cloud, Atmos. Environ., 30, 1019–1025, https://doi.org/10.1016/1352-2310(95)00409-2, 1996a.

Baechmann, K., Ebert, P., Haag, I., Prokop, T., and Steigerwald, K.: The chemical content of raindrops as a function of drop radius – II. Field experimental study on the scavenging of marked aerosol particles by raindrops sampled as a function of drop size, Atmos. Environ., 30, 1027–1033, https://doi.org/10.1016/1352-2310(95)00325-8, 1996b.

Basart, S., Nickovic, S., Terradellas, E., Cuevas, E., García-Pando, C. P., García-Castrillo, G., Werner, E., and Benincasa, F.: The WMO SDS-WAS Regional Center for Northern Africa, Middle East and Europe, E3S Web Conf., 99, 04008, https://doi.org/10.1051/e3sconf/20199904008, 2019.

Berberler, E., Gemici, B. T., Ucun Özel, H., Demir, T., and Karakaş, D.: Source identification of water-insoluble single particulate matters in rain sequences, Atmos. Pollut. Res., 13, 101499, https://doi.org/10.1016/j.apr.2022.101499, 2022.

Bertrand, G., Celle-Jeanton, H., Laj, P., Rangognio, J., and Chazot, G.: Rainfall chemistry: long range transport versus below cloud scavenging. A two-year study at an inland station (Opme, France), J. Atmos. Chem., 60, 253–271, https://doi.org/10.1007/s10874-009-9120-y, 2008.

Bukowiecki, N., Lienemann, P., Hill, M., Figi, R., Richard, A., Furger, M., Rickers, K., Falkenberg, G., Zhao, Y., and Cliff, S. S.: Real-world emission factors for antimony and other brake wear related trace elements: size-segregated values for light and heavy duty vehicles, Environ. Sci. Technol., 43, 8072–8078, 2009.

Calvo, A. I., Pont, V., Olmo, F. J., Castro, A., Alados-Arboledas, L., Vicente, A. M., Fernández-Raga, M., and Fraile, R.: Air Masses and Weather Types: A Useful Tool for Characterizing Precipitation Chemistry and Wet Deposition, Aerosol Air Qual. Res., 12, 856–878, https://doi.org/10.4209/aaqr.2012.03.0068, 2012.

Celle-Jeanton, H., Travi, Y., Loÿe-Pilot, M.-D., Huneau, F., and Bertrand, G.: Rainwater chemistry at a Mediterranean inland station (Avignon, France): Local contribution versus long-range supply, Atmos. Res., 91, 118–126, https://doi.org/10.1016/j.atmosres.2008.06.003, 2009.

Cerqueira, M., Pio, C., Legrand, M., Puxbaum, H., Kasper-Giebl, A., Afonso, J., Preunkert, S., Gelencsér, A., and Fialho, P.: Particulate carbon in precipitation at European background sites, J. Aerosol Sci., 41, 51–61, https://doi.org/10.1016/j.jaerosci.2009.08.002, 2010.

Chamberlain, A. C.: Aspects of the deposition of radioactive and other gases and particles, Int. J. Air Pollut., 3, 63–88, 1960.

Chatterjee, A., Jayaraman, A., Rao, T. N., and Raha, S.: In-cloud and below-cloud scavenging of aerosol ionic species over a tropical rural atmosphere in India, J. Atmos. Chem., 66, 27–40, https://doi.org/10.1007/s10874-011-9190-5, 2010.

Cheng, I. and Zhang, L.: Long-term air concentrations, wet deposition, and scavenging ratios of inorganic ions, $HNO_3$, and $SO_2$ and assessment of aerosol and precipitation acidity at Canadian rural locations, Atmos. Chem. Phys., 17, 4711–4730, https://doi.org/10.5194/acp-17-4711-2017, 2017.

Cheng, I., Al Mamun, A., and Zhang, L.: A synthesis review on atmospheric wet deposition of particulate elements: scavenging ratios, solubility, and flux measurements, Environ. Rev., 29, 340–353, https://doi.org/10.1139/er-2020-0118, 2021.

Colette, A., Andersson, C., Manders, A., Mar, K., Mircea, M., Pay, M.-T., Raffort, V., Tsyro, S., Cuvelier, C., Adani, M., Bessagnet, B., Bergström, R., Briganti, G., Butler, T., Cappelletti, A., Couvidat, F., D'Isidoro, M., Doumbia, T., Fagerli, H., Granier, C., Heyes, C., Klimont, Z., Ojha, N., Otero, N., Schaap, M., Sindelarova, K., Stegehuis, A. I., Roustan, Y., Vautard, R., van Meijgaard, E., Vivanco, M. G., and Wind, P.: EURODELTA-Trends, a multi-model experiment of air quality hindcast in Europe over 1990–2010, Geosci. Model Dev., 10, 3255–3276, https://doi.org/10.5194/gmd-10-3255-2017, 2017.

Croft, B., Lohmann, U., Martin, R. V., Stier, P., Wurzler, S., Feichter, J., Hoose, C., Heikkilä, U., van Donkelaar, A., and Ferrachat, S.: Influences of in-cloud aerosol scavenging parameterizations on aerosol concentrations and wet deposition in ECHAM5-HAM, Atmos. Chem. Phys., 10, 1511–1543, https://doi.org/10.5194/acp-10-1511-2010, 2010.

Dépée, A., Lemaitre, P., Gelain, T., Monier, M., and Flossmann, A.: Laboratory study of the collection efficiency of submicron aerosol particles by cloud droplets – Part I: Influence of relative humidity, Atmos. Chem. Phys., 21, 6945–6962, https://doi.org/10.5194/acp-21-6945-2021, 2021.

Desboeufs, K., Journet, E., Rajot, J.-L., Chevaillier, S., Triquet, S., Formenti, P., and Zakou, A.: Chemistry of rain events in West Africa: evidence of dust and biogenic influence in convective systems, Atmos. Chem. Phys., 10, 9283–9293, https://doi.org/10.5194/acp-10-9283-2010, 2010.

Draxler, R. R. and Rolph, G. D.: HYSPLIT (HYbrid Single-Particle Lagrangian Integrated Trajectory) Model access via NOAA ARL READY Website, http://ready.arl.noaa.gov/HYSPLIT.php (last access: 30 August 2022), 2012.

Duce, R. A., Liss, P. S., Merrill, J. T., Atlas, E. L., Buat-Menard, P., Hicks, B. B., Miller, J. M., Prospero, J. M., Arimoto, R., Church, T. M., Ellis, W., Galloway, J. N., Hansen, L., Jickells, T. D., Knap, A. H., Reinhardt, K. H., Schneider, B., Soudine, A., Tokos, J. J., Tsunogai, S., Wollast, R., and Zhou, M.: The atmospheric input of trace species to the world ocean, Global Biogeochem. Cy., 5, 193–259, https://doi.org/10.1029/91GB01778, 1991.

Favez, O., Weber, S., Petit, J.-E., Alleman, L. Y., Albinet, A., Riffault, V., Chazeau, B., Amodeo, T., Salameh, D., Zhang, Y., Srivastava, D., Samaké, A., Aujay-Plouzeau, R., Papin, A., Bonnaire, N., Boullanger, C., Chatain, M., Chevrier, F., Detournay, A., Dominik-Sègue, M., Falhun, R., Garbin, C., Ghersi, V., Grignion, G., Levigoureux, G., Pontet, S., Rangognio, J., Zhang, S., Besombes, J.-L., Conil, S., Uzu, G., Savarino, J., Marchand, N., Gros, V., Marchand, C., Jaffrezo, J.-L., and Leoz-Garziandia, E.: Overview of the French Operational Network for In Situ Observation of PM Chemical Composition and Sources in Urban Environments (CARA Program), Atmosphere, 12, 207, https://doi.org/10.3390/atmos12020207, 2021.

Ge, B., Wang, Z., Gbaguidi, A. E., and Zhang, Q.: Source Identification of Acid Rain Arising over Northeast China: Observed Evidence and Model Simulation, Aerosol Air Qual. Res., 16, 1366–1377, https://doi.org/10.4209/aaqr.2015.05.0294, 2016.

Ge, B., Xu, D., Wild, O., Yao, X., Wang, J., Chen, X., Tan, Q., Pan, X., and Wang, Z.: Inter-annual variations of wet deposition in Beijing from 2014–2017: implications of below-cloud scavenging of inorganic aerosols, Atmos. Chem. Phys., 21, 9441–9454, https://doi.org/10.5194/acp-21-9441-2021, 2021a.

Ge, Y., Heal, M. R., Stevenson, D. S., Wind, P., and Vieno, M.: Evaluation of global EMEP MSC-W (rv4.34) WRF (v3.9.1.1) model surface concentrations and wet deposition of reactive N and S with measurements, Geosci. Model Dev., 14, 7021–7046, https://doi.org/10.5194/gmd-14-7021-2021, 2021b.

Germer, S., Neill, C., Krusche, A. V., Neto, S. C. G., and Elsenbeer, H.: Seasonal and within-event dynamics of rainfall and throughfall chemistry in an open tropical rainforest in Rondônia, Brazil, Biogeochemistry, 86, 155–174, https://doi.org/10.1007/s10533-007-9152-9, 2007.

Gong, W., Stroud, C., and Zhang, L.: Cloud Processing of Gases and Aerosols in Air Quality Modeling, Atmosphere, 2, 567–616, https://doi.org/10.3390/atmos2040567, 2011.

González, C. M. and Aristizábal, B. H.: Acid rain and particulate matter dynamics in a mid-sized Andean city: The effect of rain intensity on ion scavenging, Atmos. Environ., 60, 164–171, https://doi.org/10.1016/j.atmosenv.2012.05.054, 2012.

Grythe, H., Kristiansen, N. I., Groot Zwaaftink, C. D., Eckhardt, S., Ström, J., Tunved, P., Krejci, R., and Stohl, A.: A new aerosol wet removal scheme for the Lagrangian particle model FLEXPART v10, Geosci. Model Dev., 10, 1447–1466, https://doi.org/10.5194/gmd-10-1447-2017, 2017.

Haeffelin, M., Barthès, L., Bock, O., Boitel, C., Bony, S., Bouniol, D., Chepfer, H., Chiriaco, M., Cuesta, J., Delanoë, J., Drobinski, P., Dufresne, J.-L., Flamant, C., Grall, M., Hodzic, A., Hourdin, F., Lapouge, F., Lemaître, Y., Mathieu, A., Morille, Y., Naud, C., Noël, V., O'Hirok, W., Pelon, J., Pietras, C., Protat, A., Romand, B., Scialom, G., and Vautard, R.: SIRTA, a ground-based atmospheric observatory for cloud and aerosol research, Ann. Geophys., 23, 253–275, https://doi.org/10.5194/angeo-23-253-2005, 2005.

Huff, F. A. and Stout, G. E.: Distribution of Radioactive Rainout in Convective Rainfall, J. Appl. Meteorol., 3, 707–717, 1964.

Jaffrezo, J.-L. and Colin, J.-L.: Rain-aerosol coupling in urban area: Scavenging ratio measurement and identification of some transfer processes, Atmos. Environ., 22, 929–935, https://doi.org/10.1016/0004-6981(88)90270-3, 1988.

Jaffrezo, J.-L., Colin, J.-L., and Gros, J.-M.: Some physical factors influencing scavenging ratios, Atmos. Environ. A.-Gen., 24, 3073–3083, https://doi.org/10.1016/0960-1686(90)90486-7, 1990.

Jones, A. C., Hill, A., Hemmings, J., Lemaitre, P., Quérel, A., Ryder, C. L., and Woodward, S.: Below-cloud scavenging of aerosol by rain: a review of numerical modelling approaches and sensitivity simulations with mineral dust in the Met Office's Unified Model, Atmos. Chem. Phys., 22, 11381–11407, https://doi.org/10.5194/acp-22-11381-2022, 2022.

Karşı, M. B. B., Yenísoy-Karakaş, S., and Karakaş, D.: Investigation of washout and rainout processes in sequential rain samples, Atmos. Environ., 190, 53–64, https://doi.org/10.1016/j.atmosenv.2018.07.018, 2018.

Kasahara, M., Ogiwara, H., and Yamamoto, K.: Soluble and insoluble components of air pollutants scavenged by rain water, Nucl. Instrum. Meth. B, 118, 400–402, https://doi.org/10.1016/0168-583X(95)01087-4, 1996.

Kasper-Giebl, A., Kalina, M. F., and Puxbaum, H.: Scavenging ratios for sulfate, ammonium and nitrate determined at Mt. Sonnblick (3106 m a.s.l.), Atmos. Environ., 33, 895–906, https://doi.org/10.1016/S1352-2310(98)00279-9, 1999.

Kim, K. D., Lee, S., Kim, J.-J., Lee, S.-H., Lee, D., Lee, J.-B., Choi, J.-Y., and Kim, M. J.: Effect of Wet Deposition on Secondary Inorganic Aerosols Using an Urban-Scale Air Quality Model, Atmosphere, 12, 168, https://doi.org/10.3390/atmos12020168, 2021.

Laakso, L., Grönholm, T., Rannik, Ü., Kosmale, M., Fiedler, V., Vehkamäki, H., and Kulmala, M.: Ultrafine particle scavenging coefficients calculated from 6 years field measurements, Atmos. Environ., 37, 3605–3613, https://doi.org/10.1016/S1352-2310(03)00326-1, 2003.

Laboratoire Interuniversitaire des Systèmes Atmosphériques: Data linked to the article 'Intra-event evolution of elemental and ionic concentrations in wet deposition in an urban environment', Audoux et al., ACP, 2023, http://www.lisa.u-pec.fr/fr/donnees, last access: 23 October 2023.

Laquer, F. C.: Sequential precipitation samplers: A literature review, Atmos. Environ. A.-Gen., 24, 2289–2297, https://doi.org/10.1016/0960-1686(90)90322-E, 1990.

LCSQA: Conformité technique des appareils de mesure, Laboratoire Central de Surveillance de la Qualité de l'Air, https://www.lcsqa.org/fr/conformite-technique-appareils-mesure (last access: 2 February 2023), 2021.

Lim, B., Jickells, T. D., and Davies, T. D.: Sequential sampling of particles, major ions and total trace metals in wet deposition, Atmos. Environ. A.-Gen., 25, 745–762, https://doi.org/10.1016/0960-1686(91)90073-G, 1991.

Ma, C.-J.: Chemical composition of a yellowish rainfall by the application of PIXE and micro-PIXE technique, Nuclear Instrum. Meth. B, 251, 501–506, https://doi.org/10.1016/j.nimb.2006.07.025, 2006.

Mamun, A. A., Cheng, I., Zhang, L., Celo, V., Dabek-Zlotorzynska, E., and Charland, J.-P.: Estimation of Atmospheric Dry and Wet Deposition of Particulate Elements at Four Monitoring Sites in the Canadian Athabasca Oil Sands Region, J. Geophys. Res.-Atmos., 127, e2021JD035787, https://doi.org/10.1029/2021JD035787, 2022.

Marticorena, B., Chatenet, B., Rajot, J. L., Bergametti, G., Deroubaix, A., Vincent, J., Kouoi, A., Schmechtig, C., Coulibaly, M., Diallo, A., Koné, I., Maman, A., NDiaye, T., and Zakou, A.: Mineral dust over west and central Sahel: Seasonal patterns of dry and wet deposition fluxes from a pluriannual sampling (2006–2012), J. Geophys. Res.-Atmos., 122, 1338–1364, https://doi.org/10.1002/2016JD025995, 2017.

Migliavacca, D. M., Teixeira, E. C., Raya Rodriguez, M. T., Wiegand, F., and Pereira, F. N.: Analysis of the sulfate aerosol scavenging processes in the metropolitan area of Porto Alegre (MAPA), RS, Brazil, Atmos. Pollut. Res., 1, 82–93, https://doi.org/10.5094/APR.2010.011, 2010.

Monteiro, L. R., Terzer-Wassmuth, S., Matiatos, I., Douence, C., and Wassenaar, L. I.: Distinguishing in-cloud and below-cloud short and distal N-sources from high-temporal resolution seasonal nitrate and ammonium deposition in Vienna, Austria, Atmos. Environ., 266, 118740, https://doi.org/10.1016/j.atmosenv.2021.118740, 2021.

Oduber, F., Calvo, A. I., Castro, A., Blanco-Alegre, C., Alves, C., Barata, J., Nunes, T., Lucarelli, F., Nava, S., Calzolai, G., Cerqueira, M., Martín-Villacorta, J., Esteves, V., and Fraile, R.: Chemical composition of rainwater under two events of aerosol transport: A Saharan dust outbreak and wildfires, Sci. Total Environ., 734, 139202, https://doi.org/10.1016/j.scitotenv.2020.139202, 2020.

Okita, T., Hara, H., and Fukuzaki, N.: Measurements of atmospheric $SO_2$ and $SO_4^{2-}$, and determination of the wet scavenging coefficient of sulfate aerosols for the winter monsoon season over the sea of Japan, Atmos. Environ., 30, 3733–3739, https://doi.org/10.1016/1352-2310(96)00090-8, 1996.

Pant, P. and Harrison, R. M.: Estimation of the contribution of road traffic emissions to particulate matter concentrations from field measurements: A review, Atmos. Environ., 77, 78–97, https://doi.org/10.1016/j.atmosenv.2013.04.028, 2013.

Ryu, Y.-H. and Min, S.-K.: Improving Wet and Dry Deposition of Aerosols in WRF-Chem: Updates to Below-Cloud Scavenging and Coarse-Particle Dry Deposition, J. Adv. Model. Earth Sy., 14, e2021MS002792, https://doi.org/10.1029/2021MS002792, 2022.

Seinfeld, J. H. and Pandis, S. N.: Atmospheric Chemistry and Physics: From Air Pollution to Climate Change, John Wiley & Sons, 1146 pp., ISBN 978-1-118-94740-1, 2016.

Seymour, M. D. and Stout, T.: Observations on the chemical composition of rain using short sampling times during a single event, Atmos. Environ., 17, 1483–1487, https://doi.org/10.1016/0004-6981(83)90301-3, 1983.

Slinn, W. G. N.: Some approximations for the wet and dry removal of particles and gases from the atmosphere, Water, Air Soil Pollut., 7, 513–543, https://doi.org/10.1007/BF00285550, 1977.

Sparmacher, H., Fülber, K., and Bonka, H.: Below-cloud scavenging of aerosol particles: Particle-bound radionuclides–Experimental, Atmos. Environ. A-Gen., 27, 605–618, https://doi.org/10.1016/0960-1686(93)90218-N, 1993.

Tanner, P. A., Tam, C. W. F., Tanner, P. A., and Tam, C. W. F.: In-Cloud Concentrations and Below-Cloud Scavenging Processes in Hong Kong, China, Environ. Chem., 3, 142–148, https://doi.org/10.1071/EN05084, 2006.

Tapiador, F. J., Checa, R., and de Castro, M.: An experiment to measure the spatial variability of rain drop size distribution using sixteen laser disdrometers, Geophys. Res. Lett., 37, L16803, https://doi.org/10.1029/2010GL044120, 2010.

Taylor, S. R. and McLennan, S. M.: The continental crust: Its composition and evolution, ISBN 0632011483, 1985.

Thorpe, A. and Harrison, R. M.: Sources and properties of non-exhaust particulate matter from road traffic: A review, Sci. Total Environ., 400, 270–282, https://doi.org/10.1016/j.scitotenv.2008.06.007, 2008.

Vincent, J., Laurent, B., Losno, R., Bon Nguyen, E., Roullet, P., Sauvage, S., Chevaillier, S., Coddeville, P., Ouboulmane, N., di Sarra, A. G., Tovar-Sánchez, A., Sferlazzo, D., Massanet, A., Triquet, S., Morales Baquero, R., Fornier, M., Coursier, C., Desboeufs, K., Dulac, F., and Bergametti, G.: Variability of mineral dust deposition in the western Mediterranean basin and south-east of France, Atmos. Chem. Phys., 16, 8749–8766, https://doi.org/10.5194/acp-16-8749-2016, 2016.

Wang, X., Zhang, L., and Moran, M. D.: Uncertainty assessment of current size-resolved parameterizations for below-cloud particle scavenging by rain, Atmos. Chem. Phys., 10, 5685–5705, https://doi.org/10.5194/acp-10-5685-2010, 2010.

Wang, X., Zhang, L., and Moran, M. D.: On the discrepancies between theoretical and measured below-cloud particle scavenging coefficients for rain – a numerical investigation using a detailed one-dimensional cloud microphysics model, Atmos. Chem. Phys., 11, 11859–11866, https://doi.org/10.5194/acp-11-11859-2011, 2011.

Wang, X., Zhang, L., and Moran, M. D.: Development of a new semi-empirical parameterization for below-cloud scavenging of size-resolved aerosol particles by both rain and snow, Geosci. Model Dev., 7, 799–819, https://doi.org/10.5194/gmd-7-799-2014, 2014.

Wiegand, F., Pereira, F. N., and Teixeira, E. C.: Study on wet scavenging of atmospheric pollutants in south Brazil, Atmos. Environ., 45, 4770–4776, https://doi.org/10.1016/j.atmosenv.2010.02.020, 2011.

Xu, D., Ge, B., Wang, Z., Sun, Y., Chen, Y., Ji, D., Yang, T., Ma, Z., Cheng, N., Hao, J., and Yao, X.: Below-cloud wet scavenging of soluble inorganic ions by rain in Beijing during the summer of 2014, Environ. Pollut., 230, 963–973, https://doi.org/10.1016/j.envpol.2017.07.033, 2017.

Xu, D., Ge, B., Chen, X., Sun, Y., Cheng, N., Li, M., Pan, X., Ma, Z., Pan, Y., and Wang, Z.: Multi-method determination of the below-cloud wet scavenging coefficients of aerosols in Beijing, China, Atmos. Chem. Phys., 19, 15569–15581, https://doi.org/10.5194/acp-19-15569-2019, 2019.

Yamagata, S., Kobayashi, D., Ohta, S., Murao, N., Shiobara, M., Wada, M., Yabuki, M., Konishi, H., and Yamanouchi, T.: Properties of aerosols and their wet deposition in the arctic spring during ASTAR2004 at Ny-Alesund, Svalbard, Atmos. Chem. Phys., 9, 261–270, https://doi.org/10.5194/acp-9-261-2009, 2009.

Yang, Q., Easter, R. C., Campuzano-Jost, P., Jimenez, J. L., Fast, J. D., Ghan, S. J., Wang, H., Berg, L. K., Barth, M. C., Liu, Y., Shrivastava, M. B., Singh, B., Morrison, H., Fan, J., Ziegler, C. L., Bela, M., Apel, E., Diskin, G. S., Mikoviny, T., and Wisthaler, A.: Aerosol transport and wet scavenging in deep convective clouds: A case study and model evaluation using a multiple passive tracer analysis approach, J. Geophys. Res.-Atmos., 120, 8448–8468, https://doi.org/10.1002/2015JD023647, 2015.

Zou, C., Yang, X., Zhang, Y., and Huang, H.: Characteristics and distribution of inorganic ions in segmented precipitation and contribution of below-cloud/in-cloud scavenging in Nanchang, Air Qual. Atmos. Hlth., 15, 903–916, https://doi.org/10.1007/s11869-022-01166-3, 2022.